Computers and Mathematics with Applications 126 (2022) 31–42

Contents lists available at ScienceDirect

Computers and Mathematics with Applications

www.elsevier.com/locate/camwa

A mixed virtual element method for Biot's consolidation model

Feng Wang [a,*,1], Mingchao Cai [b,2], Gang Wang [c,3], Yuping Zeng [d,4]

[a] Jiangsu Key Laboratory for NSLSCS, School of Mathematical Sciences, Nanjing Normal University, Nanjing 210023, China
[b] Department of Mathematics, Morgan State University, Baltimore, MD 21251, USA
[c] The Department of Applied Mathematics, Northwestern Polytechnical University, Xi'an 710072, China
[d] School of Mathematics, Jiaying University, Meizhou 514015, China

ARTICLE INFO

Keywords:
Poroelasticity equations
Virtual element methods
Weak Galerkin

ABSTRACT

In this paper, we shall present a weak virtual element method for the standard three field poroelasticity problem on polytopal meshes. The flux velocity and pressure are approximated by the low order $\mathbf{H}(\mathrm{div})$ virtual element and the piecewise constant, while the elastic displacement is discretized by the $\mathbf{H}(\mathrm{div})$ virtual element with some tangential polynomials on element boundaries. A fully discrete scheme is then given by choosing the backward Euler for the time discretization. With some assumptions on the exact solutions, we prove that the convergence order is of order 1 with respect to the meshsize and the time step, and the hidden constants are independent of the parameters of the problems. Some numerical experiments are given to verify the results.

1. Introduction

In the field of petroleum engineering, the interaction of the fluid flow and elastic porous medium is described by the Biot consolidation model, stated as

$$\begin{cases} -\operatorname{div}\sigma(\boldsymbol{u})+\alpha\nabla p=\boldsymbol{f}_{\boldsymbol{u}}, & in\ \Omega\times(0,T),\\ \kappa^{-1}\boldsymbol{w}+\nabla p=\boldsymbol{f}_{\boldsymbol{w}}, & in\ \Omega\times(0,T),\\ c_0p_t+\alpha\operatorname{div}\boldsymbol{u}_t+\operatorname{div}\boldsymbol{w}=f_p, & in\ \Omega\times(0,T), \end{cases} \tag{1}$$

with the initial conditions $p(\cdot,0)=p_0$, $\boldsymbol{u}(\cdot,0)=\boldsymbol{u}_0$. The subscript t stands for the derivative with respect to the time variable t. We impose the boundary conditions $\boldsymbol{u}=\mathbf{0}$, $\boldsymbol{w}\cdot\boldsymbol{n}=0$ for ease of presentation. Here, $\Omega\subset\mathbb{R}^d, d=2,3$, is assumed to be a polygonal or polyhedral domain. The variables $\boldsymbol{u}$, $\boldsymbol{w}$, p stand for the displacement of the solid, velocity and pressure of the fluid respectively. We use $\sigma(\boldsymbol{u})=2\mu\epsilon(\boldsymbol{u})+\lambda\operatorname{div}\boldsymbol{u}\mathbb{I}$ to denote the effective stress, where λ and μ are Lamé constants. The notation κ is the hydraulic conductivity and assumed to be a constant. The coefficient α is the Biot-Willis constant, which couples the elastic and Darcy's equations and is usually close to unity. The parameter $c_0\geq 0$ stands for the constrained specific storage coefficient.

This model is of increasing importance and of great interest due to its applications in various fields including biomechanics, soil mechanics, geophysics, physical chemistry and material sciences. There have been lots of literature on numerical methods for the poroelasticity problem, see, e.g., [26–28] for coupling the mixed finite element and the continuous/discontinuous Galerkin methods, [38,18] for combining the mixed and nonconforming finite element method, [34] for a weak Galerkin method coupled with the mixed finite element method. One can also refer to [22,3] and the references therein for iterative coupling methods.

In the numerical simulations of Biot's model, there are mainly two difficulties people should overcome. One is to avoid nonphysical fluid pressure oscillations (see [16,29,31] and references therein) for a certain range of material parameters, e.g., $c_0=0$, low permeabilities and/or small time steps. To this end, some stabilized methods were pro-

* Corresponding author.
E-mail addresses: fengwang@live.cn (F. Wang), cmchao2005@gmail.com (M. Cai), gangwang.math@nwpu.edu.cn (G. Wang), zeng_yuping@163.com (Y. Zeng).

[1] The first author is supported in part by the National Natural Science Foundation of China (Nos. 12071227, 11871281), the Natural Science Foundation of the Jiangsu Higher Education Institutions of China (No. 20KJA110001), and the Ministry of Science and Technology of China (No. 2020YFA0713800).
[2] The second author is supported in part by NIH-BUILD grant through UL1GM118973, NIH-RCMI grant through U54MD013376, and the National Science Foundation awards (1700328, 1831950).
[3] The third author is supported by the Fundamental Research Funds for the Central Universities (No. G2019KY05104) and the National Natural Science Foundation of China (No. 12001433).
[4] The fourth author is supported by the Guangdong Basic and Applied Basic Research Foundation (Grant Nos. 2018A030307024 and 2020A1515011032), and the National Natural Science Foundation of China (Grant No. 11526097).

https://doi.org/10.1016/j.camwa.2022.09.005
Received 16 March 2022; Received in revised form 25 August 2022; Accepted 4 September 2022

posed in [32,6,30,33,24]. The other one is to deal with the notorious volume locking phenomenon when $\lambda \to \infty$. Oyarzúa and Ruiz-Baier [25] introduced a pseudo total pressure and proposed a new three field formulation to obtain a stable and robust method for a static problem. We refer to [20] for a similar formulation and its preconditioners. Feng et al. [15] presented a reformulation of the original model by introducing two pseudo-pressures and developed a robust full discrete finite element scheme. In [40], Yi studied the causes of Poisson locking and pressure oscillation, and proposed a new discrete mixed form by employing the method of reduced integration to the bilinear form of the displacement. Using specific parameter-dependent norms, Hong and Kraus [17] established the full parameter-robust inf-sup stability of the three field continuous problem, and proposed a uniformly stable discretization method. Based on a four field formulation, Yi and Lee [39,19,2] also independently developed convergent finite element methods which are robust with respect to the parameters c_0 and λ.

In the last few years, due to the great flexibility for problems on complicated geometry (see, e.g., [11] for interface problems), numerical methods on polytopal meshes have drawn increasingly attentions. Several methods have been proposed, such as, mimetic finite difference methods [21], virtual element methods (VEM) [4], weak Galerkin methods [37], hybrid high order methods [14], generalized barycentric coordinates method (e.g., [12]) and so on. There are only few work discussed the discretization of the Biot model based on polytopal meshes. In [7], Boffi et al. constructed a coupling of a discontinuous Galerkin and a hybrid high-order method on general polyhedral meshes. It was shown that the stability and error estimates hold when the specific storage coefficient vanishes and depend mildly on the heterogeneity of the permeability coefficients. In [13], the authors combined the first-order VEM and the finite volume method for the poroelasticity. The first fully VEM discretization for the Biot model problem was given in [9]. Their robust scheme combines with the H^1 conforming VEM proposed in [1] for the displacement, piecewise constant approximations for total pressure, and the enhanced H^1 virtual element space for the pore pressure. Based on the displacement, fluid flux and pressure formulation, Tang et al. [36] combined a lowest H^1-conforming VEM enriched with normal bubbles on edges and a pair of mixed VEM to obtain a locking-free scheme. They also discussed the virtual element approximate method of order $k \geq 2$.

In this paper, we shall present a new virtual element method on polygonal/polyhedral meshes for the problem (1). To approximate the flux and pressure variables, we apply the H(div) virtual element [5] and the piecewise constant, which is the same as the ones used in [36]. For the displacement, instead of enriching the low-order H^1 conforming virtual element used in [36,9], we directly start with the H(div) virtual element [5] which is continuous along the normal direction of element boundaries and thus strongly mass-conservative. To compute the (weak) gradient, we additionally involve a tangential direction space on each element face, and define a weak symmetric gradient to approximate the symmetric gradient by a dual argument [37]. We use the backward Euler method for the time discretization and propose a fully discrete scheme. Error analysis is given to show the convergence order of the proposed method is optimal. Moreover, it is shown that the error bounds are independent of the Lamé constant λ and the constrained specific storage coefficient c_0. Our method has a unified formulation for both two and three dimensional problems. Although, we only consider the low order space element, it can be extended to the k-th order space element [10] naturally.

The paper is organized as follows. In Section 2, we introduce the virtual element spaces and some notations. Section 3 concerns with the semidiscrete problem. The fully discrete method is given in Section 4. In Section 5, we report some numerical experiments to verify our results.

Throughout the paper, we use bold letters to denote vector variables, operators, and spaces. We use P_k or $\boldsymbol{P}_k$ to indicate the polynomial space of the polynomials or vector polynomials up to order k. For any region D, $(\cdot,\cdot)_D$ (or $\langle\cdot,\cdot\rangle_D$) denotes the L^2 or $\boldsymbol{L}^2$ inner product. The norm and seminorm for the functions in the scalar Sobolev space $H^m(D)$ or $\boldsymbol{H}^m(D)$ $(m \geq 0)$ are denoted by $\|\cdot\|_{m,D}$ and $|\cdot|_{m,D}$ respectively. When $m=0$, we usually omit the subscript and use $\|\cdot\|_D$ to denote the L^2 (or $\boldsymbol{L}^2$) norm. When D stands for the whole domain Ω, we drop the subscript Ω in the norms and inner products. We also use $\boldsymbol{H}(\mathrm{div})$ and $\boldsymbol{H}(\mathbf{curl})$ to denote the Sobolev spaces, in which the functions and their divergence and **curl** are in L^2 and $\boldsymbol{L}^2$ spaces, respectively. Additionally, the notation $\lesssim$ abbreviates an inequality $\leq$ up to a constant which is independent of the mesh size and the parameters c_0, λ.

2. H(div) virtual element spaces

Let $\mathcal{T}_h$ be a partition of Ω into non-overlapping polygons/polyhedrons. In this paper, we assume that each element in $\mathcal{T}_h$ is shape regular, that is, (i) each element $E \in \mathcal{T}_h$ and its edges/faces are star shaped, (ii) the diameters of the edges/faces and elements are equivalent $h_f \simeq h_E$. Furthermore, we suppose the diameters of all the elements are of comparable size denoted by h, which means that the mesh is quasi-uniform. All the faces are denoted by $\mathcal{F}_h$.

We first introduce the $\boldsymbol{H}(\mathrm{div})$ virtual element proposed in [5]. For ease of presentation, we only focus on the lowest order element. Given a polyhedron E, define

$$\boldsymbol{W}_E = \Big\{ \boldsymbol{v} \in \boldsymbol{H}(\mathrm{div}) \cap \boldsymbol{H}(\mathbf{curl}) : \boldsymbol{v}\cdot\boldsymbol{n} \in P_1(f)\ \forall f \subset \partial E,\quad \mathrm{div}\,\boldsymbol{v} \in P_0(E),\ \mathbf{curl}\,\boldsymbol{v} \in \boldsymbol{P}_0(E) \Big\}.$$

It is obvious that $\boldsymbol{W}_E$ not only contains all the linear functions, but also non-polynomial functions, which is the reason called virtual element space. The degree of freedoms for functions in $\boldsymbol{W}_E$ are stated as

$$\int_f \boldsymbol{v}\cdot\boldsymbol{n} q \quad \forall\, q \in P_1(f), f \subset \partial E, \tag{2}$$

$$\int_E \boldsymbol{v}\cdot\boldsymbol{q} \quad \forall\, \boldsymbol{q} \in \boldsymbol{P}_1(E) \setminus \nabla P_2(E). \tag{3}$$

The unisolvence can be found in [5]. Although the functions in $\boldsymbol{W}_E$ have no explicit expressions, their projections to the vector linear space are computable via the definition of the degree of freedoms (see [5, Section 3.5] for details), i.e., one can define an $\boldsymbol{L}^2$ projection $\boldsymbol{\Pi}_E^o : \boldsymbol{W}_E \to \boldsymbol{P}_1(E)$ as

$$\int_E \boldsymbol{\Pi}_E^o \boldsymbol{v} \cdot \boldsymbol{q} := \int_E \boldsymbol{v} \cdot \boldsymbol{q} \quad \forall \boldsymbol{q} \in \boldsymbol{P}_1(E).$$

Next, on each face f of E, we introduce a space $\boldsymbol{V}_f := \boldsymbol{P}_0(f) + \mathbf{RM}(f)$, where $\mathbf{RM}(f)$ denotes the space of rigid motions on f. We note that $\boldsymbol{V}_f$ is the constant space in two dimensions. Let $\boldsymbol{\tau}_i, i = 1, \cdots, d-1$, be the orthogonal unit tangential vectors on the face. Then, each vector $\boldsymbol{v}$ in $\boldsymbol{P}_1(f)$ can be expressed as the summation of the tangential component, i.e., $\boldsymbol{v} = \sum_{i=1}^{d-1} v_i \boldsymbol{\tau}_i,\ v_i \in P_1(f)$. The facewise $\boldsymbol{L}^2$ projection to $\boldsymbol{V}_f$ is denoted by $\boldsymbol{\Pi}_{\partial E}^{\boldsymbol{\tau}} \boldsymbol{v}$. It is easy to see

$$\boldsymbol{\Pi}_{\partial E}^{\boldsymbol{\tau}}(\boldsymbol{v}\cdot\boldsymbol{\tau}_i \boldsymbol{\tau}_i) = \boldsymbol{\Pi}_{\partial E}^{\boldsymbol{\tau}}(\boldsymbol{v})\cdot\boldsymbol{\tau}_i \boldsymbol{\tau}_i, \quad (\boldsymbol{\Pi}_{\partial E}^{\boldsymbol{\tau}} \boldsymbol{v}) \cdot \boldsymbol{n} = 0.$$

We also use $\boldsymbol{\Pi}_{\partial E}$ to involve both of the normal and tangential components, that is,

$$\boldsymbol{\Pi}_{\partial E} \boldsymbol{v} := \boldsymbol{v}\cdot\boldsymbol{n}\boldsymbol{n} + \boldsymbol{\Pi}_{\partial E}^{\boldsymbol{\tau}} \boldsymbol{v}.$$

Then, a local weak virtual element space on E is defined as

$$\boldsymbol{V}_E := \Big\{ \boldsymbol{v}_E = \{\boldsymbol{v}_E^{\mathrm{div}}, \boldsymbol{v}_e^t\}, \boldsymbol{v}_E^{\mathrm{div}} \in \boldsymbol{W}_E, \boldsymbol{v}_e^t|_f \in \boldsymbol{V}_f, f \subset \partial E \Big\}.$$

This element is used to approximate the $\boldsymbol{H}^1$ functions. To impose the gradient operator on the functions in $\boldsymbol{V}_E$, we introduce a weak gradient proposed in [23,37]. For any $\boldsymbol{v} = \{\boldsymbol{v}^{\mathrm{div}}, \boldsymbol{v}^{\boldsymbol{\tau}}\} \in \boldsymbol{V}_E$, define $\nabla_E^w \boldsymbol{v} \in \mathbb{P}_0(E)$ as a constant matrix satisfying

$$(\nabla_E^w \boldsymbol{v}, \mathbb{W})_E := \langle \boldsymbol{v}^{\text{div}} \cdot \boldsymbol{n}, \mathbb{W}\boldsymbol{n}\cdot\boldsymbol{n}\rangle_{\partial E} + \sum_{i=1}^{d-1} \langle \boldsymbol{v}^{\boldsymbol{\tau}} \cdot \boldsymbol{\tau}_i, \mathbb{W}\boldsymbol{n}\cdot\boldsymbol{\tau}_i\rangle_{\partial E} \tag{4}$$

for all $\mathbb{W}$ in $\mathbb{P}_0(E)$. Then the weak symmetric gradient is defined as

$$\boldsymbol{\epsilon}_E^w(\boldsymbol{v}) = (\nabla_E^w \boldsymbol{v} + (\nabla_E^w \boldsymbol{v})^{\boldsymbol{\tau}})/2.$$

Let $\mathcal{J}_{\partial E}^{\boldsymbol{n}}(\boldsymbol{v})$ and $\mathcal{J}_{\partial E}^{\boldsymbol{\tau}_i}(\boldsymbol{v})$ denote the differences of $\boldsymbol{v} \in \boldsymbol{V}_E$ and $\boldsymbol{\Pi}_E^o \boldsymbol{v}$ in normal and tangential directions respectively, that is,

$$\mathcal{J}_{\partial E}^{\boldsymbol{n}}(\boldsymbol{v}) := (\boldsymbol{v}^{\text{div}} - \boldsymbol{\Pi}_E^o \boldsymbol{v}^{\text{div}})\cdot \boldsymbol{n}\boldsymbol{n}, \quad \mathcal{J}_{\partial E}^{\boldsymbol{\tau}_i}(\boldsymbol{v}) := (\boldsymbol{v}^{\boldsymbol{\tau}} - \boldsymbol{\Pi}_E^o \boldsymbol{v}^{\text{div}})\cdot \boldsymbol{\tau}_i \boldsymbol{\tau}_i.$$

When the superscript is omitted, it indicates the whole jump on the element boundary

$$\mathcal{J}_{\partial E}(\boldsymbol{v}) := \mathcal{J}_{\partial E}^{\boldsymbol{n}}(\boldsymbol{v}) + \mathcal{J}_{\partial E}^{\boldsymbol{\tau}}(\boldsymbol{v}),$$

where $\mathcal{J}_{\partial E}^{\boldsymbol{\tau}}(\boldsymbol{v}) := \sum_{i=1}^{d-1} \mathcal{J}_{\partial E}^{\boldsymbol{\tau}_i}(\boldsymbol{v})$.

By the $\boldsymbol{L}^2$ projections and integration by parts, the definition (4) can be stated as

$$(\nabla_E^w \boldsymbol{v}, \mathbb{W})_E = (\nabla(\boldsymbol{\Pi}_E^o \boldsymbol{v}), \mathbb{W})_E + \langle \boldsymbol{\Pi}_{\partial E} \mathcal{J}_{\partial E}(\boldsymbol{v}), \mathbb{W}\boldsymbol{n}\rangle_{\partial E},$$

which means that $\nabla_E^w \boldsymbol{v}$ is just the standard gradient $\nabla(\boldsymbol{\Pi}_E^o \boldsymbol{v})$ plus contributions from the boundary. Therefore, with the assumption of the element, we obtain by the Schwarz inequality, the trace theorem, and the inverse inequality, that

$$\|\nabla(\boldsymbol{\Pi}_E^o \boldsymbol{v}) - \nabla_E^w(\boldsymbol{v})\|_E^2 \lesssim h^{-1} \|\boldsymbol{\Pi}_{\partial E} \mathcal{J}_{\partial E}(\boldsymbol{v})\|_{\partial E}^2. \tag{5}$$

We also need to define interpolations to the virtual element space. For any $\boldsymbol{v} \in \boldsymbol{H}^1(E)$, $\boldsymbol{I}_E^{\boldsymbol{W}} \boldsymbol{v} \in \boldsymbol{W}_E$ is defined by the degree of freedoms in (2)-(3), i.e.,

$$\int_f \boldsymbol{I}_E^{\boldsymbol{W}} \boldsymbol{v}\cdot \boldsymbol{n} q = \int_f \boldsymbol{v}\cdot \boldsymbol{n} q \quad q \in P_1(f), f \subset \partial E,$$

$$\int_E \boldsymbol{I}_E^{\boldsymbol{W}} \boldsymbol{v}\cdot \boldsymbol{q} = \int_E \boldsymbol{v}\cdot \boldsymbol{q} \quad \boldsymbol{q} \in \boldsymbol{P}_1(E) \setminus \nabla P_2(E).$$

The interpolation $\boldsymbol{I}_E^{\boldsymbol{V}}$ to the space $\boldsymbol{V}_E$ is defined as $\boldsymbol{I}_E^{\boldsymbol{V}} \boldsymbol{v} := \{\boldsymbol{I}_E^{\boldsymbol{W}} \boldsymbol{v}, \boldsymbol{\Pi}_{\partial E}^{\boldsymbol{\tau}} \boldsymbol{v}\}$. By the scaling argument and the Bramble-Hilbert theorem, we have the following estimates for the projection and interpolation.

Lemma 2.1. *Assume that $E \in \mathcal{T}_h$ is shape regular. Then for all $\boldsymbol{v} \in \boldsymbol{H}^2(E)$, it is true that*

$$\|\boldsymbol{v} - \boldsymbol{I}_E^{\boldsymbol{W}} \boldsymbol{v}\|_E \lesssim h^m \|\boldsymbol{v}\|_{m,E}, \ m = 1, 2, \tag{6}$$

$$\|\boldsymbol{v} - \boldsymbol{\Pi}_E^o \boldsymbol{v}\|_E + h\|\nabla(\boldsymbol{v} - \boldsymbol{\Pi}_E^o \boldsymbol{v})\|_E \lesssim h^m \|\boldsymbol{v}\|_{m,E}, \ m = 1, 2, \tag{7}$$

$$\|\boldsymbol{v} - \boldsymbol{\Pi}_E^o \boldsymbol{I}_E^{\boldsymbol{W}} \boldsymbol{v}\|_E + h\|\nabla(\boldsymbol{v} - \boldsymbol{\Pi}_E^o \boldsymbol{I}_E^{\boldsymbol{W}} \boldsymbol{v})\|_E \lesssim h^m \|\boldsymbol{v}\|_{m,E}, \ m = 1, 2, \tag{8}$$

$$\|\boldsymbol{\Pi}_{\partial E}^{\boldsymbol{\tau}} \mathcal{J}_{\partial E}^{\boldsymbol{\tau}}(\boldsymbol{I}_E^{\boldsymbol{V}} \boldsymbol{v})\|_{\partial E} + \|\boldsymbol{v} - \boldsymbol{\Pi}_E^o \boldsymbol{I}_E^{\boldsymbol{V}} \boldsymbol{v}\|_{\partial E} \lesssim h^{\frac{3}{2}} \|\boldsymbol{v}\|_{2,E}. \tag{9}$$

The virtual element space for the flux is stated as

$$\boldsymbol{W}_h := \{\boldsymbol{v} \in \boldsymbol{H}(\text{div}), \boldsymbol{v}|_E \in \boldsymbol{W}_E, \forall E \in \mathcal{T}_h, \boldsymbol{v}\cdot \boldsymbol{n} = 0 \text{ on } \partial\Omega\},$$

while for the displacement, we use the weak virtual element space

$$\boldsymbol{V}_h := \left\{ \boldsymbol{v}_h = \{\boldsymbol{v}_h^{\text{div}}, \boldsymbol{v}_h^{\boldsymbol{\tau}}\}, \boldsymbol{v}_h^{\text{div}} \in \boldsymbol{W}_h, \boldsymbol{v}_h^{\boldsymbol{\tau}}|_f \in \boldsymbol{V}_f, \boldsymbol{v}^{\boldsymbol{\tau}} = \boldsymbol{0} \text{ on } \partial\Omega \right\}.$$

We also use a discontinuous piecewise constant element space $Q_h \subset L_0^2(\Omega)$ to discretize the pressure, and use I_h^Q to denote the L^2 projection to Q_h.

When the subscript E is replaced by the mesh size h, the operators introduced above are element-wise defined on the whole domain, i.e., $(\boldsymbol{\epsilon}_h^w(\cdot))|_E = \boldsymbol{\epsilon}_E^w(\cdot)$, $\boldsymbol{\Pi}_h^o|_E = \boldsymbol{\Pi}_E^o$, $\boldsymbol{I}_h^{\boldsymbol{W}}|_E = \boldsymbol{I}_E^{\boldsymbol{W}}$, $\boldsymbol{I}_h^{\boldsymbol{V}}|_E = \boldsymbol{I}_E^{\boldsymbol{V}}$. We also use $\epsilon_h(\boldsymbol{v})$ and $\nabla_h \boldsymbol{v}$ to stand for the element-wise symmetric gradient and gradient of $\boldsymbol{v}$ in $\boldsymbol{V}_h$.

3. The semidiscrete problem

In this section, we first present the semidiscrete problem, and then show the error estimates.

Given $\boldsymbol{u}_h(0) = \boldsymbol{I}_h^{\boldsymbol{V}} \boldsymbol{u}_0$, $p_h(0) = I_h^Q p_0$, the corresponding discrete variational formulation for the problem (1) is to seek $\boldsymbol{u}_h \in \boldsymbol{V}_h$, $\boldsymbol{w}_h \in \boldsymbol{W}_h$, and $p_h \in Q_h$ satisfying

$$\begin{cases} a_{h,1}(\boldsymbol{u}_h, \boldsymbol{v}_h) - b_1(\boldsymbol{v}_h, p_h) = (\boldsymbol{f}_{\boldsymbol{u}}, \boldsymbol{\Pi}_h^o \boldsymbol{v}_h) & \forall\, \boldsymbol{v}_h \in \boldsymbol{V}_h, \\ a_{h,2}(\boldsymbol{w}_h, \boldsymbol{z}_h) - b_2(\boldsymbol{z}_h, p_h) = (\boldsymbol{f}_{\boldsymbol{w}}, \boldsymbol{\Pi}_h^o \boldsymbol{z}_h) & \forall\, \boldsymbol{z}_h \in \boldsymbol{W}_h, \\ b_1(\boldsymbol{u}_{ht}, q_h) + b_2(\boldsymbol{w}_h, q_h) + a_{h,3}(p_{ht}, q_h) = (f_p, q_h) & \forall\, q_h \in Q_h, \end{cases} \tag{10}$$

where

$$a_{h,1}(\boldsymbol{u}_h, \boldsymbol{v}_h) := (2\mu \boldsymbol{\epsilon}_h^w(\boldsymbol{u}_h), \boldsymbol{\epsilon}_h^w(\boldsymbol{v}_h)) + \lambda(\text{div}\, \boldsymbol{u}_h, \text{div}\, \boldsymbol{v}_h) + 2\ \mu s_1(\boldsymbol{u}_h, \boldsymbol{v}_h),$$

$$a_{h,2}(\boldsymbol{w}_h, \boldsymbol{z}_h) := (\kappa^{-1} \boldsymbol{\Pi}_h^o \boldsymbol{w}_h, \boldsymbol{\Pi}_h^o \boldsymbol{z}_h) + \kappa^{-1} s_2(\boldsymbol{w}_h, \boldsymbol{z}_h),$$

$$a_{h,3}(p_h, q_h) := (c_0 p_h, q_h),$$

$$b_1(\boldsymbol{v}_h, p_h) := \alpha(\text{div}\, \boldsymbol{v}_h, p_h), \quad b_2(\boldsymbol{z}_h, p_h) := (\text{div}\, \boldsymbol{z}_h, p_h),$$

with the stabilization term defined as

$$s_1(\boldsymbol{u}_h, \boldsymbol{v}_h) := \sum_{E \in \mathcal{T}_h} h^{-1} \Big\langle \boldsymbol{\Pi}_{\partial E} \mathcal{J}_{\partial E}(\boldsymbol{u}_h), \boldsymbol{\Pi}_{\partial E} \mathcal{J}_{\partial E}(\boldsymbol{v}_h) \Big\rangle_{\partial E},$$

$$s_2(\boldsymbol{w}_h, \boldsymbol{z}_h) := \mathcal{D}^E((I - \boldsymbol{\Pi}_h^o)\boldsymbol{w}_h, (I - \boldsymbol{\Pi}_h^o)\boldsymbol{z}_h),$$

where $\mathcal{D}^E$ is corresponding to the identity operator with respect to the local basis determined by the degrees of freedom (2)-(3), see [8] for details. It is shown that (see [8])

$$a_{h,2}(\boldsymbol{z}_h, \boldsymbol{z}_h) \simeq (\kappa^{-1} \boldsymbol{z}_h, \boldsymbol{z}_h). \tag{11}$$

By the bilinear forms, we define norms (semi-norms) for any $\boldsymbol{v}_h \in \boldsymbol{V}_h$ and $\boldsymbol{z} \in \boldsymbol{W}_h$ as

$$\|\boldsymbol{v}_h\|_{a_1} = \sqrt{a_{h,1}(\boldsymbol{v}_h, \boldsymbol{v}_h)}, \ \|\boldsymbol{z}_h\|_{a_2} = \sqrt{a_{h,2}(\boldsymbol{z}_h, \boldsymbol{z}_h)}.$$

Let ρ be a positive constant. Then a weighted norm is defined as

$$\|\phi\|_{m,\rho} := \|\rho^{\frac{1}{2}} \phi\|_m \quad \forall\ \phi \in H^m \text{ or } \boldsymbol{H}^m, m = 0, 1.$$

On each element E, we introduce a seminorm for $\boldsymbol{v}_h \in \boldsymbol{V}_E$ as

$$\|\boldsymbol{v}_h\|_{1,h,E}^2 := \|\nabla \boldsymbol{\Pi}_E^o \boldsymbol{v}_h\|_E^2 + \|h^{-\frac{1}{2}} \boldsymbol{\Pi}_{\partial E} \mathcal{J}_{\partial E}(\boldsymbol{v}_h)\|_{\partial E}^2,$$

and thus, a mesh dependent seminorm for all $\boldsymbol{v}_h \in \boldsymbol{V}_h$ is stated as

$$\|\boldsymbol{v}_h\|_{1,h}^2 := \sum_{E \in \mathcal{T}_h} \|\boldsymbol{v}_h\|_{1,h,E}^2. \tag{12}$$

It can be shown that, on $\boldsymbol{V}_h$, $\|\cdot\|_{1,h}$ and $\|\cdot\|_{a_1}$ are norms and the bilinear form $a_{h,1}(\cdot,\cdot)$ is coercive, see [10, Lemma 3.7] for details.

Lemma 3.1. *Provided the element E is shape regular, we have for all $\boldsymbol{v} \in \boldsymbol{V}_E$ that*

$$\|\boldsymbol{v} - \boldsymbol{\Pi}_E^o \boldsymbol{v}\|_E^2 \lesssim h \|\mathcal{J}_{\partial E}^{\boldsymbol{n}}(\boldsymbol{v})\|_{\partial E}^2. \tag{13}$$

Proof. This inequality follows from the definition of $\boldsymbol{\Pi}_E^o$, the scaling arguments and the assumption of the mesh regularity. □

Lemma 3.2. *Assume the mesh $\mathcal{T}_h$ is quasi-uniform. For any $p_h \in Q_h$, there exists a $\boldsymbol{z}_h \in \boldsymbol{W}_h$ and a $\boldsymbol{v}_h = \{\boldsymbol{v}_h^{\text{div}}, \boldsymbol{v}_h^{\boldsymbol{\tau}}\} \in \boldsymbol{V}_h$ such that*

$$\text{div}\, \boldsymbol{z}_h = \text{div}\, \boldsymbol{v}_h = p_h, \qquad \|\boldsymbol{z}_h\|_0 \lesssim \|p_h\|_0, \quad \text{and} \quad \|\boldsymbol{v}_h\|_{1,h} \lesssim \|p_h\|_0.$$

Proof. We refer to [8, Theorem 5.4] and [10, Lemma 12] for the proof. □

Theorem 3.3. *There exists a unique solution to the problem (10).*

Proof. Our proof follows the idea in [26]. For completeness, we present the outline. First, we introduce some operators associated with the bilinear forms, that is, $A_1 : \boldsymbol{V}_h \to \boldsymbol{V}'_h$, $A_2 : \boldsymbol{W}_h \to \boldsymbol{W}'_h$, $A_3 : Q_h \to Q'_h$, $B_1 : \boldsymbol{V}_h \to Q'_h$, $B_2 : \boldsymbol{W}_h \to Q'_h$ satisfying

$$(A_1\boldsymbol{u}_h, \boldsymbol{v}_h) = a_{h,1}(\boldsymbol{u}_h, \boldsymbol{v}_h),\ (A_2\boldsymbol{w}_h, \boldsymbol{z}_h) = a_{h,2}(\boldsymbol{w}_h, \boldsymbol{z}_h),$$

$$(A_3 p_h, q_h) = a_{h,3}(p_h, q_h),\ (B_1\boldsymbol{v}_h, q_h) = b_1(\boldsymbol{v}_h, q_h),\ (B_2\boldsymbol{z}_h, q_h) = b_2(\boldsymbol{z}_h, q_h).$$

Then the problem (10) can be rewritten as

$$\begin{aligned} A_1\boldsymbol{u}_h - B_1^T p_h &= F_1,\\ A_2\boldsymbol{w}_h - B_2^T p_h &= F_2,\\ B_1\boldsymbol{u}_{ht} + B_2\boldsymbol{w}_h + A_3 p_{ht} &= F_3, \end{aligned}$$

where F_1, F_2, F_3 are the operators corresponding to the right hand side. Note that A_1 and A_2 are symmetric and positive definite. Taking the derivate with respect to t in the first equation, and using direct calculation, we have

$$(A_3 + B_1A_1^{-1}B_1^T)p_{ht} + B_2A_2^{-1}B_2^T p_h = F_3 - B_2A_2^{-1}F_2 - B_1A_1^{-1}F_{1t}.$$

From the theory of ODE, there is a unique p_h satisfying the above equation, provided that the operator $A_3 + B_1A_1^{-1}B_1^T$ is invertible and the other operators are bounded. □

Lemma 3.4. *If $\boldsymbol{u} \in \boldsymbol{H}^2(E)$ and E is shape regular, we have*

$$\|\epsilon(\boldsymbol{u}) - \epsilon_E^w(\boldsymbol{I}_h^{\boldsymbol{V}}\boldsymbol{u})\|_E + h\|\epsilon(\boldsymbol{u}) - \epsilon_E^w(\boldsymbol{I}_h^{\boldsymbol{V}}\boldsymbol{u})\|_{1,E} + h^{-\frac{1}{2}}\|\boldsymbol{\Pi}_{\partial E}\mathcal{J}_{\partial E}(\boldsymbol{I}_h^{\boldsymbol{V}}\boldsymbol{u})\|_{\partial E}$$
$$\lesssim h\|\boldsymbol{u}\|_{2,E}.$$

Proof. In view of (5), (7), and (9), we obtain the desired inequality. □

Lemma 3.5. *On each shape regular element $E \in \mathcal{T}_h$, we have for any $\boldsymbol{p} \in \boldsymbol{P}_k(E)$ that*

$$\|\boldsymbol{p} - \boldsymbol{\Pi}_{\partial E}^{\tau}\boldsymbol{p}\|_{\partial E} \lesssim h^{\frac{1}{2}}\|\epsilon(\boldsymbol{p})\|_E.$$

Proof. This inequality follows from the Korn inequality up to rigid motions contained in the face spaces, see, e.g., [10]. □

Lemma 3.6. *Assume the mesh is quasi-uniform. It is true for any $\boldsymbol{v}_h = \{\boldsymbol{v}_h^{\mathrm{div}}, \boldsymbol{v}_h^{\tau}\} \in \boldsymbol{V}_h$ that*

$$\|\mathcal{J}_{\partial E}(\boldsymbol{v}_h)\|_{\partial E}^2 \lesssim \|\boldsymbol{\Pi}_{\partial E}\mathcal{J}_{\partial E}(\boldsymbol{v}_h)\|_{\partial E}^2 + h\|\epsilon(\boldsymbol{\Pi}_E^o\boldsymbol{v}_h)\|_E^2 \le h\|\boldsymbol{v}_h\|_{1,h}^2. \tag{14}$$

Proof. By the triangle inequality and Lemma 3.5, we have the first inequality, and then the second one. □

We next give the error analysis for the semidiscrete problem (10). Let $(\boldsymbol{u}, \boldsymbol{w}, p)$ and $(\boldsymbol{u}_h, \boldsymbol{w}_h, p_h)$ be the solutions to problems (1) and (10) respectively. We define the errors as

$$\theta_{\boldsymbol{u}} := \boldsymbol{I}_h^{\boldsymbol{V}}\boldsymbol{u} - \boldsymbol{u}_h, \theta_{\boldsymbol{w}} := \boldsymbol{I}_h^{\boldsymbol{W}}\boldsymbol{w} - \boldsymbol{w}_h, \theta_p = I_h^Q p - p_h.$$

It is obvious that the initial error $\theta_{\boldsymbol{u}}(\cdot,0) = \boldsymbol{0}$ and $\theta_p(\cdot,0) = 0$. By the definition of the virtual element spaces and projection I_h^Q, we have $b_1(\boldsymbol{v}_h, p - I_h^Q p) = b_1(\boldsymbol{v}_h, p - I_h^Q p) = 0$. Then we have the following error equations.

Lemma 3.7. *It is true for the errors that*

$$a_{h,1}(\theta_{\boldsymbol{u}}, \boldsymbol{v}_h) - b_1(\boldsymbol{v}_h, \theta_p) = \mathcal{R}_1(\boldsymbol{v}_h) \quad \forall \boldsymbol{v}_h \in \boldsymbol{V}_h, \tag{15}$$

$$a_{h,2}(\theta_{\boldsymbol{w}}, \boldsymbol{z}_h) - b_2(\boldsymbol{z}_h, \theta_p) = \mathcal{R}_2(\boldsymbol{z}_h) \quad \forall \boldsymbol{z}_h \in \boldsymbol{W}_h, \tag{16}$$

$$b_1(\theta_{\boldsymbol{u}_t}, q_h) + b_2(\theta_{\boldsymbol{w}}, q_h) + a_{h,3}(\theta_{p_t}, q_h) = 0 \quad \forall q_h \in Q_h, \tag{17}$$

where

$$\begin{aligned} \mathcal{R}_1(\boldsymbol{v}_h) :=& (\boldsymbol{f}_{\boldsymbol{u}}, \boldsymbol{v}_h - \boldsymbol{\Pi}_h^o\boldsymbol{v}_h) + 2\,\mu s_1(\boldsymbol{I}_h^{\boldsymbol{V}}\boldsymbol{u}, \boldsymbol{v}_h)\\ &+ 2\mu(\epsilon_h^w(\boldsymbol{I}_h^{\boldsymbol{V}}\boldsymbol{u}), \epsilon_h^w(\boldsymbol{v}_h)) + 2\mu(\mathrm{div}(\epsilon(\boldsymbol{u})), \boldsymbol{v}_h),\\ \mathcal{R}_2(\boldsymbol{z}_h) :=& (\boldsymbol{f}_{\boldsymbol{w}}, \boldsymbol{z}_h - \boldsymbol{\Pi}_h^o\boldsymbol{z}_h) + a_{h,2}(\boldsymbol{I}_h^{\boldsymbol{W}}\boldsymbol{w}, \boldsymbol{z}_h) - (\kappa^{-1}\boldsymbol{w}, \boldsymbol{z}_h). \end{aligned}$$

Moreover, taking time derivative of (15) and (16) leads to

$$a_{h,1}(\theta_{\boldsymbol{u}_t}, \boldsymbol{v}_h) - b_1(\boldsymbol{v}_h, \theta_{p_t}) = \mathcal{R}_{1t}(\boldsymbol{v}_h) \quad \forall \boldsymbol{v}_h \in \boldsymbol{V}_h, \tag{18}$$

$$a_{h,2}(\theta_{\boldsymbol{w}_t}, \boldsymbol{z}_h) - b_2(\boldsymbol{z}_h, \theta_{p_t}) = \mathcal{R}_{2t}(\boldsymbol{z}_h) \quad \forall \boldsymbol{z}_h \in \boldsymbol{W}_h, \tag{19}$$

where

$$\begin{aligned} \mathcal{R}_{1t}(\boldsymbol{v}_h) :=& (\boldsymbol{f}_{\boldsymbol{u}t}, \boldsymbol{v}_h - \boldsymbol{\Pi}_h^o\boldsymbol{v}_h) + 2\,\mu s_1(\boldsymbol{I}_h^{\boldsymbol{V}}\boldsymbol{u}_t, \boldsymbol{v}_h)\\ &+ 2\mu(\epsilon_h^w(\boldsymbol{I}_h^{\boldsymbol{V}}\boldsymbol{u}_t), \epsilon_h^w(\boldsymbol{v}_h)) + 2\mu(\mathrm{div}(\epsilon(\boldsymbol{u}_t)), \boldsymbol{v}_h),\\ \mathcal{R}_{2t}(\boldsymbol{z}_h) :=& (\boldsymbol{f}_{\boldsymbol{w}t}, \boldsymbol{z}_h - \boldsymbol{\Pi}_h^o\boldsymbol{z}_h) + a_{h,2}(\boldsymbol{I}_h^{\boldsymbol{W}}\boldsymbol{w}_t, \boldsymbol{z}_h) - (\kappa^{-1}\boldsymbol{w}_t, \boldsymbol{z}_h). \end{aligned}$$

Here $\boldsymbol{f}_{\boldsymbol{u}t} := \frac{\mathrm{d}\boldsymbol{f}_{\boldsymbol{u}}}{\mathrm{dt}}$, $\boldsymbol{f}_{\boldsymbol{w}t} := \frac{\mathrm{d}\boldsymbol{f}_{\boldsymbol{w}}}{\mathrm{dt}}$.

Lemma 3.8. *If the mesh is quasi-uniform, and $\boldsymbol{f}_{\boldsymbol{u}} \in \boldsymbol{L}^2$, $\boldsymbol{w} \in \boldsymbol{H}^1$, $\boldsymbol{u} \in \boldsymbol{H}^2$, $\boldsymbol{f}_{\boldsymbol{w}} \in \boldsymbol{H}_h^1$, which denotes the piecewise $\boldsymbol{H}^1$ space, we have the following consistency errors:*

$$\mathcal{R}_1(\boldsymbol{v}_h) \lesssim h\mu^{\frac{1}{2}}M_{\boldsymbol{u}}^{\frac{1}{2}}\|\boldsymbol{v}_h\|_{1,h} \le hM_{\boldsymbol{u}}^{\frac{1}{2}}\|\boldsymbol{v}_h\|_{a_1} \quad \forall \boldsymbol{v}_h \in \boldsymbol{V}_h, \tag{20}$$

$$\mathcal{R}_2(\boldsymbol{z}_h) \lesssim hM_{\boldsymbol{w}}^{\frac{1}{2}}\|\boldsymbol{z}_h\|_{a_2} \quad \forall \boldsymbol{z}_h \in \boldsymbol{W}_h, \tag{21}$$

where $M_{\boldsymbol{u}} := \|\boldsymbol{f}_{\boldsymbol{u}}\|_{0,\mu^{-1}} + \|\boldsymbol{u}\|_{2,\mu}$, $M_{\boldsymbol{w}} := \|\kappa^{\frac{1}{2}}\boldsymbol{f}_{\boldsymbol{w}}\|_{h,1} + \|\boldsymbol{w}\|_{1,\kappa^{-1}}$, and $\|\cdot\|_{h,1}$ denotes the broken $\boldsymbol{H}^1$ norm with respect to the partition $\mathcal{T}_h$. Similarly, provided $\boldsymbol{f}_{\boldsymbol{u}t} \in \boldsymbol{L}^2$, $\boldsymbol{w}_t \in \boldsymbol{H}^1$, $\boldsymbol{u}_t \in \boldsymbol{H}^2$, $\boldsymbol{f}_{\boldsymbol{w}t} \in \boldsymbol{H}_h^1$, it holds that

$$\mathcal{R}_{1t}(\boldsymbol{v}_h) \lesssim hM_{\boldsymbol{u}t}^{\frac{1}{2}}\|\boldsymbol{v}_h\|_{a_1}, \quad \mathcal{R}_{2t}(\boldsymbol{z}_h) \lesssim hM_{\boldsymbol{w}t}^{\frac{1}{2}}\|\boldsymbol{z}_h\|_{a_2} \tag{22}$$

with the constant defined as $M_{\boldsymbol{u}t} = \|\boldsymbol{f}_{\boldsymbol{u}t}\|_{0,\mu^{-1}} + \|\boldsymbol{u}_t\|_{2,\mu}$ and $M_{\boldsymbol{w}t} = \|\kappa^{\frac{1}{2}}\boldsymbol{f}_{\boldsymbol{w}t}\|_{h,1} + \|\boldsymbol{w}_t\|_{1,\kappa^{-1}}$.

Proof. We estimate the error term by term. It follows from the property of the $\boldsymbol{L}^2$ projection (13) that

$$(\boldsymbol{f}_{\boldsymbol{u}}, \boldsymbol{v}_h - \boldsymbol{\Pi}_h^o\boldsymbol{v}_h) \le \|\boldsymbol{f}_{\boldsymbol{u}}\|_0\|\boldsymbol{v}_h - \boldsymbol{\Pi}_h^o\boldsymbol{v}_h\|_0 \lesssim h\|\boldsymbol{f}_{\boldsymbol{u}}\|_0\|\boldsymbol{v}_h\|_{1,h}.$$

For the stabilized term s_1, it follows from the Cauchy-Schwarz inequality and Lemma 3.4 that

$$\begin{aligned} s_1(\boldsymbol{I}_h^{\boldsymbol{V}}\boldsymbol{u}, \boldsymbol{v}_h) &= \sum_{E\in\mathcal{T}_h} h^{-1}\left\langle \boldsymbol{\Pi}_{\partial E}\mathcal{J}_{\partial E}(\boldsymbol{I}_h^{\boldsymbol{V}}\boldsymbol{u}), \boldsymbol{\Pi}_{\partial E}\mathcal{J}_{\partial E}(\boldsymbol{v}_h)\right\rangle_{\partial E}\\ &\le \sum_{E\in\mathcal{T}_h} h^{-1}\|\boldsymbol{\Pi}_{\partial E}\mathcal{J}_{\partial E}(\boldsymbol{I}_h^{\boldsymbol{V}}\boldsymbol{u})\|_{\partial E}\|\boldsymbol{\Pi}_{\partial E}\mathcal{J}_{\partial E}(\boldsymbol{v}_h)\|_{\partial E}\\ &\lesssim h\|\boldsymbol{u}\|_2\|\boldsymbol{v}\|_{1,h}. \end{aligned}$$

Integration by parts and the definition of ϵ_h^w gives

$$\begin{aligned} &(\epsilon_h^w(\boldsymbol{I}_h^{\boldsymbol{V}}\boldsymbol{u}), \epsilon_h^w(\boldsymbol{v}_h)) + (\mathrm{div}(\epsilon(\boldsymbol{u})), \boldsymbol{v}_h)\\ &= \left((I - \boldsymbol{\Pi}_h^o)\,\mathrm{div}\,\epsilon(\boldsymbol{u}), (\boldsymbol{\Pi}_h^o - I)\boldsymbol{v}_h\right) + \sum_{E\in\mathcal{T}_h}\langle(\epsilon(\boldsymbol{u}) - \epsilon_h^w(\boldsymbol{I}_h^{\boldsymbol{V}}\boldsymbol{u}))\boldsymbol{n}, \mathcal{J}_{\partial E}(\boldsymbol{v}_h)\rangle_{\partial E}, \end{aligned}$$

which, together with Lemmas 3.4 and 3.6, yields

$$(\epsilon_h^w(\boldsymbol{I}_h^{\boldsymbol{V}}\boldsymbol{u}), \epsilon_h^w(\boldsymbol{v}_h)) + (\mathrm{div}(\epsilon(\boldsymbol{u})), \boldsymbol{v}_h) \lesssim h\|\boldsymbol{u}\|_2\|\boldsymbol{v}_h\|_{1,h}.$$

The inequality (20) follows directly from the above three inequalities.
For the inequality (21), we derive by the inequalities (6)-(8) that

$$(\boldsymbol{f}_{\boldsymbol{w}}, \boldsymbol{z}_h - \boldsymbol{\Pi}_h^o \boldsymbol{z}_h) \leq (\boldsymbol{f}_{\boldsymbol{w}} - \boldsymbol{\Pi}_h^o \boldsymbol{f}_{\boldsymbol{w}}, \boldsymbol{z}_h) \lesssim h \|\boldsymbol{f}_{\boldsymbol{w}}\|_{h,1} \|\boldsymbol{z}_h\|_0,$$
$$s_2(\boldsymbol{I}_h^{\boldsymbol{W}} \boldsymbol{w}, \boldsymbol{z}_h) \lesssim \|(I - \boldsymbol{\Pi}_h^o)\boldsymbol{I}_h^{\boldsymbol{W}} \boldsymbol{w}\|_0 \|(I - \boldsymbol{\Pi}_h^o)\boldsymbol{z}_h\|_0 \lesssim h \|\boldsymbol{w}\|_1 \|\boldsymbol{z}_h\|_0,$$

and

$$\begin{aligned}(\boldsymbol{\Pi}_h^o(\boldsymbol{I}_h^{\boldsymbol{W}} \boldsymbol{w}), \boldsymbol{\Pi}_h^o \boldsymbol{z}_h) - (\boldsymbol{w}, \boldsymbol{z}_h) &= (\boldsymbol{w} - \boldsymbol{\Pi}_h^o \boldsymbol{w}, \boldsymbol{\Pi}_h^o \boldsymbol{z}_h - \boldsymbol{z}_h) \\ &\quad + (\boldsymbol{\Pi}_h^o(\boldsymbol{I}_h^{\boldsymbol{W}} \boldsymbol{w}) - \boldsymbol{w}, \boldsymbol{\Pi}_h^o \boldsymbol{z}_h) \\ &\lesssim h \|\boldsymbol{w}\|_1 \|\boldsymbol{z}_h\|_0.\end{aligned}$$

Thus, we have

$$\mathcal{R}_2(\boldsymbol{z}_h) \lesssim h(\|\kappa^{\frac{1}{2}} \boldsymbol{f}_{\boldsymbol{w}}\|_{h,1} + \|\boldsymbol{w}\|_{1,\kappa^{-1}}) \|\boldsymbol{z}_h\|_{a_2}.$$

The proof of (22) is similar, and we omit it here. The proof is completed. □

Lemma 3.9. *Under the assumption in Lemma 3.8, we have*

$$\|\theta_p\|_0^2 \lesssim \mu \alpha^{-2}(\|\theta_{\boldsymbol{u}}\|_{a_1}^2 + h^2 M_{\boldsymbol{u}}). \tag{23}$$

Similarly, it also holds that

$$\|\theta_p\|_0^2 \lesssim \kappa^{-1}(\|\theta_{\boldsymbol{w}}\|_{a_2}^2 + h^2 M_{\boldsymbol{w}}). \tag{24}$$

Proof. It follows from Lemma 3.2 that there exists a $\boldsymbol{v}_h \in \boldsymbol{V}_h$ such that

$$\operatorname{div} \boldsymbol{v}_h = \alpha^{-1}\theta_p, \quad \|\boldsymbol{v}_h\|_{1,h} \lesssim \alpha^{-1}\|\theta_p\|_0.$$

Then, we deduce that

$$\begin{aligned}\|\theta_p\|_0^2 &= (\alpha \operatorname{div} \boldsymbol{v}_h, \theta_p) = a_{h,1}(\theta_{\boldsymbol{u}}, \boldsymbol{v}_h) - \mathcal{R}_1(\boldsymbol{v}_h) \\ &\lesssim \mu \|\theta_{\boldsymbol{u}}\|_{1,h} \|\boldsymbol{v}_h\|_{1,h} + h\mu^{\frac{1}{2}} M_{\boldsymbol{u}}^{\frac{1}{2}} \|\boldsymbol{v}_h\|_{1,h} \\ &\lesssim \alpha^{-1}\mu^{\frac{1}{2}}(\|\theta_{\boldsymbol{u}}\|_{a_1} + hM_{\boldsymbol{u}}^{\frac{1}{2}})\|\theta_p\|_0.\end{aligned}$$

We note that, in the first inequality, we have used the fact that $(\operatorname{div}(\boldsymbol{I}_h^{\boldsymbol{V}} \boldsymbol{u} - \boldsymbol{u}), \operatorname{div} \boldsymbol{v}_h) = 0$. The proof is completed. □

Theorem 3.10. *Let $(\boldsymbol{u}, \boldsymbol{w}, p)$ and $(\boldsymbol{u}_h, \boldsymbol{w}_h, p_h)$ be the unique solutions to (1) and (10) respectively. Additionally, assume that $\boldsymbol{u} \in L^\infty(\boldsymbol{H}^2)$, $\boldsymbol{u}_t \in L^1(\boldsymbol{H}^2)$, $\boldsymbol{f}_{\boldsymbol{u}} \in L^\infty(\boldsymbol{L}^2)$, $\boldsymbol{f}_{\boldsymbol{u}t} \in L^1(\boldsymbol{L}^2)$, $\boldsymbol{w} \in L^1(\boldsymbol{H}^1)$, $\boldsymbol{f}_{\boldsymbol{w}} \in L^1(\boldsymbol{H}_h^1)$. We have*

$$\sup_{0\leq t\leq T} \|\boldsymbol{I}_h^{\boldsymbol{V}} \boldsymbol{u} - \boldsymbol{u}_h\|_{a_1}^2 \lesssim h^2 e^t \left(\sup_{0\leq t\leq T} M_{\boldsymbol{u}} + \int_0^T M_1 \, \mathrm{d}t \right), \tag{25}$$

$$\int_0^t \|\boldsymbol{I}_h^{\boldsymbol{W}} \boldsymbol{w} - \boldsymbol{w}_h\|_{a_2}^2 \, \mathrm{d}t \lesssim h^2(1 + Te^T) \left(\sup_{0\leq t\leq T} M_{\boldsymbol{u}} + \int_0^T M_1 \, \mathrm{d}t \right), \tag{26}$$

$$\sup_{0\leq t\leq T} \|I_h^Q p - p_h\|_0^2 \lesssim h^2 \mu \alpha^{-2} e^T \left(\sup_{0\leq t\leq T} M_{\boldsymbol{u}} + \int_0^T M_1 \, \mathrm{d}t \right), \tag{27}$$

where the constant M_1 stands for $M_{\boldsymbol{u}_t} + M_{\boldsymbol{w}}$. Furthermore, if $\boldsymbol{w} \in L^\infty(\boldsymbol{H}^1)$, $\boldsymbol{f}_{\boldsymbol{w}} \in L^\infty(\boldsymbol{H}_h^1)$, $\boldsymbol{w}_t \in L^1(\boldsymbol{H}^1)$, $\boldsymbol{f}_{\boldsymbol{w}t} \in L^1(\boldsymbol{H}_h^1)$, it is true that

$$\sup_{0\leq t\leq T} \|\boldsymbol{I}_h^{\boldsymbol{W}} \boldsymbol{w} - \boldsymbol{w}_h\|_{a_2}^2 \lesssim e^T \left(\|\theta_{\boldsymbol{w}}(0)\|_{a_2}^2 + h^2 \int_0^T M_t \, \mathrm{d}t \right), \tag{28}$$

$$\sup_{0\leq t\leq T} \|I_h^Q p - p_h\|_{0,\kappa}^2 \lesssim e^T \left(\|\theta_{\boldsymbol{w}}(0)\|_{a_2}^2 + h^2 \sup_{0\leq t\leq T} M_{\boldsymbol{w}} + h^2 \int_0^T M_t \, \mathrm{d}t \right), \tag{29}$$

where $M_t := M_{\boldsymbol{u}t} + M_{\boldsymbol{w}t}$.

Proof. Setting $\boldsymbol{v}_h = \theta_{\boldsymbol{u}_t}$, $\boldsymbol{z}_h = \theta_{\boldsymbol{w}}$, and $q_h = \theta_p$ in Lemma 3.7, we derive that

$$\begin{aligned}&a_{h,1}(\theta_{\boldsymbol{u}}, \theta_{\boldsymbol{u}_t}) + a_{h,2}(\theta_{\boldsymbol{w}}, \theta_{\boldsymbol{w}}) + (c_0\theta_{p_t}, \theta_p) \\ &= a_{h,1}(\theta_{\boldsymbol{u}}, \theta_{\boldsymbol{u}_t}) - b_1(\theta_{\boldsymbol{u}_t}, \theta_p) + a_{h,2}(\theta_{\boldsymbol{w}}, \theta_{\boldsymbol{w}}) - b_2(\theta_{\boldsymbol{w}}, \theta_p) \\ &\quad + b_1(\theta_{\boldsymbol{u}_t}, \theta_p) + b_2(\theta_{\boldsymbol{w}}, \theta_p) + (c_0\theta_{p_t}, \theta_p) \\ &= \mathcal{R}_1(\theta_{\boldsymbol{u}_t}) + \mathcal{R}_2(\theta_{\boldsymbol{w}}).\end{aligned}$$

Integration in time from 0 to t gives

$$\frac{1}{2}\|\theta_{\boldsymbol{u}}\|_{a_1}^2 + \frac{1}{2}c_0\|\theta_p\|_0^2 + \int_0^t \|\theta_{\boldsymbol{w}}\|_{a_2}^2 \, \mathrm{d}t = \int_0^t \mathcal{R}_1(\theta_{\boldsymbol{u}_t}) \, \mathrm{d}t + \int_0^t \mathcal{R}_2(\theta_{\boldsymbol{w}}) \, \mathrm{d}t. \tag{30}$$

We first consider the term $\int_0^t \mathcal{R}_1(\theta_{\boldsymbol{u}_t}) \, \mathrm{d}t$. Using integration by parts and Lemma 3.8, we derive that

$$\begin{aligned}\int_0^t \mathcal{R}_1(\theta_{\boldsymbol{u}_t}) \, \mathrm{d}t &= \mathcal{R}_1(\theta_{\boldsymbol{u}})\Big|_0^t - \int_0^t \mathcal{R}_{1t}(\theta_{\boldsymbol{u}}) \, \mathrm{d}t \\ &\leq ChM_{\boldsymbol{u}}^{\frac{1}{2}} \|\theta_{\boldsymbol{u}}\|_{a_1} + h \int_0^t M_{\boldsymbol{u}t}^{\frac{1}{2}} \|\theta_{\boldsymbol{u}}\|_{a_1} \, \mathrm{d}t \\ &\leq Ch^2 M_{\boldsymbol{u}} + \frac{1}{4}\|\theta_{\boldsymbol{u}}\|_{a_1}^2 + Ch^2 \int_0^t M_{\boldsymbol{u}t} \, \mathrm{d}t + \int_0^t \|\theta_{\boldsymbol{u}}\|_{a_1}^2 \, \mathrm{d}t.\end{aligned} \tag{31}$$

For the term $\int_0^t \mathcal{R}_2(\theta_{\boldsymbol{w}}) \, \mathrm{d}t$, it follows from Lemma 3.8 and the Cauchy-Schwarz inequality that

$$\begin{aligned}\int_0^t \mathcal{R}_2(\theta_{\boldsymbol{w}}) \, \mathrm{d}t &\leq Ch \int_0^t M_{\boldsymbol{w}}^{\frac{1}{2}} \|\theta_{\boldsymbol{w}}\|_{a_2} \, \mathrm{d}t \\ &\leq Ch^2 \int_0^t M_{\boldsymbol{w}} \, \mathrm{d}t + \frac{1}{2}\int_0^t \|\theta_{\boldsymbol{w}}\|_{a_2}^2 \, \mathrm{d}t.\end{aligned} \tag{32}$$

Plugging the above two inequalities into (30), we obtain

$$\begin{aligned}&\frac{1}{4}\|\theta_{\boldsymbol{u}}\|_{a_1}^2 + \frac{1}{2}c_0\|\theta_p\|^2 + \frac{1}{2}\int_0^t \|\theta_{\boldsymbol{w}}\|_{a_2}^2 \, \mathrm{d}t \\ &\leq \int_0^t \|\theta_{\boldsymbol{u}}\|_{a_1}^2 \, \mathrm{d}t + Ch^2 \left(M_{\boldsymbol{u}} + \int_0^t M_1 \, \mathrm{d}t \right),\end{aligned}$$

which, together with the Gronwall inequality, gives

$$\|\theta_{\boldsymbol{u}}\|_{a_1}^2 \lesssim h^2 e^t \left(M_{\boldsymbol{u}} + \int_0^t M_1 \, \mathrm{d}t \right), \tag{33}$$

and then, we arrive at the other two inequalities (26) and (27) from (33) and (23).

We next set $\boldsymbol{v}_h = \theta_{\boldsymbol{u}_t}$, $\boldsymbol{z}_h = \theta_{\boldsymbol{w}}$ and $q_h = \theta_{p_t}$ in (18), (19), and (17), to have

$$\begin{aligned}&a_{h,1}(\theta_{\boldsymbol{u}_t}, \theta_{\boldsymbol{u}_t}) + a_{h,2}(\theta_{\boldsymbol{w}_t}, \theta_{\boldsymbol{w}}) + (c_0\theta_{p_t}, \theta_{p_t}) = \mathcal{R}_{1t}(\theta_{\boldsymbol{u}_t}) + \mathcal{R}_{2t}(\theta_{\boldsymbol{w}}) \\ &\lesssim hM_{\boldsymbol{u}t}^{\frac{1}{2}} \|\theta_{\boldsymbol{u}_t}\|_{a_1} + hM_{\boldsymbol{w}t}^{\frac{1}{2}} \|\theta_{\boldsymbol{w}}\|_{a_2} \\ &\leq Ch^2(M_{\boldsymbol{u}t} + M_{\boldsymbol{w}t}) + \frac{1}{2}\|\theta_{\boldsymbol{u}_t}\|_{a_1}^2 + \frac{1}{2}\|\theta_{\boldsymbol{w}}\|_{a_2}^2.\end{aligned}$$

Thereby, we obtain

$$\frac{1}{2}\frac{\mathrm{d}\|\theta_{\boldsymbol{w}}\|_{a_2}^2}{\mathrm{d}t} = a_{h,2}(\theta_{\boldsymbol{w}_t},\theta_{\boldsymbol{w}}) \le Ch^2(M_{\boldsymbol{u}t}+M_{\boldsymbol{w}t}) + \|\theta_{\boldsymbol{w}}\|_{a_2}^2.$$

Integration in time from 0 to t gives

$$\|\theta_{\boldsymbol{w}}\|_{a_2}^2 \le \|\theta_{\boldsymbol{w}}(0)\|_{a_2}^2 + Ch^2\int_0^t (M_{\boldsymbol{u}t}+M_{\boldsymbol{w}t})\,\mathrm{d}t + \int_0^t \|\theta_{\boldsymbol{w}}\|_{a_2}^2\,\mathrm{d}t.$$

Then the inequality (28) follows from the Gronwall inequality, and the inequality (29) is obtained directly from (24). The proof is completed. □

Remark 3.11. From the inequality (26), we take $T \to 0$ and obtain

$$\|\boldsymbol{I}_h^{\boldsymbol{W}}\boldsymbol{w}(0)-\boldsymbol{w}_h(0)\|_{a_2}^2 \lesssim h^2(M_{\boldsymbol{u}}(0)+M_1(0)),$$

and thus the inequalities (28) and (29) can be rewritten as

$$\sup_{0\le t\le T}\|\boldsymbol{I}_h^{\boldsymbol{W}}\boldsymbol{w}-\boldsymbol{w}_h\|_{a_2}^2 \lesssim h^2 e^T\left(M_{\boldsymbol{u}}(0)+M_1(0)+\int_0^T M_t\,\mathrm{d}t\right),$$

$$\sup_{0\le t\le T}\|I_h^Q p - p_h\|_{0,\kappa}^2 \lesssim h^2 e^T\left(M_{\boldsymbol{u}}(0)+M_1(0)+\sup_{0\le t\le T}M_{\boldsymbol{w}}+\int_0^T M_t\,\mathrm{d}t\right).$$

4. Fully discrete scheme

Let $\Delta t = T/N$ be a uniform time step size, and $t^n = n\Delta t, 0\le n\le N$ be the discrete times. The notation δ_t stands for the backward Euler time discretization, i.e.,

$$\delta_t \boldsymbol{u}^n := \frac{\boldsymbol{u}^n-\boldsymbol{u}^{n-1}}{\Delta t},\quad \delta_t p^n := \frac{p^n-p^{n-1}}{\Delta t},$$

where $\boldsymbol{u}^n = \boldsymbol{u}(\cdot,t^n)$, $p^n = p(\cdot,t^n)$. We always use superscript n to denote the functions at the time t^n.

Then, given $\boldsymbol{u}_h^0 = \boldsymbol{I}_h^{\boldsymbol{V}}\boldsymbol{u}_0$, $p_h^0 = I_h^Q p_0$, the corresponding fully discrete scheme is to seek $\boldsymbol{u}_h^n\in\boldsymbol{V}_h$, $\boldsymbol{w}_h^n\in\boldsymbol{W}_h$, and $p_h^n\in Q_h$ satisfying

$$\begin{cases} a_{h,1}(\boldsymbol{u}_h^n,\boldsymbol{v}_h)-b_1(\boldsymbol{v}_h,p_h^n)=(\boldsymbol{f}_{\boldsymbol{u}}^n,\boldsymbol{\Pi}_h^o\boldsymbol{v}_h) & \forall\,\boldsymbol{v}_h\in\boldsymbol{V}_h,\\ a_{h,2}(\boldsymbol{w}_h^n,\boldsymbol{z}_h)-b_2(\boldsymbol{z}_h,p_h^n)=(\boldsymbol{f}_{\boldsymbol{w}}^n,\boldsymbol{\Pi}_h^o\boldsymbol{z}_h) & \forall\,\boldsymbol{z}_h\in\boldsymbol{W}_h,\\ b_1(\delta_t\boldsymbol{u}_h^n,q_h)+b_2(\boldsymbol{w}_h^n,q_h)+a_{h,3}(\delta_t p_h^n,q_h)=(f_p^n,q_h) & \forall\,q_h\in Q_h.\end{cases} \tag{34}$$

In view of the quasi-uniform assumption of the mesh, there exists a unique pair of solution at each time.

At each discrete time t^n, we denote the errors as

$$\theta_{\boldsymbol{u}}^n := \boldsymbol{I}_h^{\boldsymbol{V}}\boldsymbol{u}^n-\boldsymbol{u}_h^n, \theta_{\boldsymbol{w}}^n := \boldsymbol{I}_h^{\boldsymbol{W}}\boldsymbol{w}^n-\boldsymbol{w}_h^n, \theta_p^n := I_h^Q p^n - p_h^n.$$

Similarly as Lemma 3.7, the error equations at each discrete time are stated as follows.

$$a_{h,1}(\theta_{\boldsymbol{u}}^n,\boldsymbol{v}_h)-b_1(\boldsymbol{v}_h,\theta_p^n)=\mathcal{R}_1^n(\boldsymbol{v}_h)\quad \forall\boldsymbol{v}_h\in\boldsymbol{V}_h, \tag{35}$$

$$a_{h,2}(\theta_{\boldsymbol{w}}^n,\boldsymbol{z}_h)-b_2(\boldsymbol{z}_h,\theta_p^n)=\mathcal{R}_2^n(\boldsymbol{z}_h)\quad \forall\boldsymbol{z}_h\in\boldsymbol{W}_h, \tag{36}$$

$$b_1(\delta_t\theta_{\boldsymbol{u}}^n,q_h)+b_2(\theta_{\boldsymbol{w}}^n,q_h)+a_{h,3}(\delta_t\theta_p^n,q_h)=\mathcal{R}_3^n(q_h)\quad \forall q_h\in Q_h, \tag{37}$$

where

$$\begin{aligned}\mathcal{R}_1^n(\boldsymbol{v}_h) &:= (\boldsymbol{f}_{\boldsymbol{u}}^n,\boldsymbol{v}_h-\boldsymbol{\Pi}_h^o\boldsymbol{v}_h)+2\,\mu s_1(\boldsymbol{I}_h^{\boldsymbol{V}}\boldsymbol{u}^n,\boldsymbol{v}_h)\\ &\quad +2\mu(\epsilon_h^{w}(\boldsymbol{I}_h^{\boldsymbol{V}}\boldsymbol{u}^n),\epsilon_h^{w}(\boldsymbol{v}_h))+2\mu(\mathrm{div}(\epsilon(\boldsymbol{u}^n)),\boldsymbol{v}_h),\\ \mathcal{R}_2^n(\boldsymbol{z}_h) &:= (\boldsymbol{f}_{\boldsymbol{w}}^n,\boldsymbol{z}_h-\boldsymbol{\Pi}_h^o\boldsymbol{z}_h)+a_{h,2}(\boldsymbol{I}_h^{\boldsymbol{W}}\boldsymbol{w}^n,\boldsymbol{z}_h)-(\kappa^{-1}\boldsymbol{w}^n,\boldsymbol{z}_h),\\ \mathcal{R}_3^n(q_h) &:= b_1(\delta_t\boldsymbol{u}^n-\boldsymbol{u}_t^n,q_h)+a_{h,3}(\delta_t p^n-p_t^n,q_h).\end{aligned}$$

Lemma 4.1. *Assume $\boldsymbol{u}_t\in L^2(\boldsymbol{H}^2)$, $\boldsymbol{f}_{\boldsymbol{u}t}\in L^2(\boldsymbol{L}^2)$ and the mesh is quasi-uniform, it is true that*

$$\mathcal{R}_1^n(\boldsymbol{v}_h^n)-\mathcal{R}_1^{n-1}(\boldsymbol{v}_h^n)\lesssim Ch^2\int_{t^{n-1}}^{t^n} M_{\boldsymbol{u}t}\,\mathrm{d}t+\frac{\Delta t}{8}\|\boldsymbol{v}_h^n\|_{a_1}^2\quad \forall\boldsymbol{v}_h^n\in\boldsymbol{V}_h. \tag{38}$$

Proof. By the definitions of $\mathcal{R}_1^n$ and $\mathcal{R}_{1t}$, we observe that

$$\begin{aligned}\mathcal{R}_1^n(\boldsymbol{v}_h^n)-\mathcal{R}_1^{n-1}(\boldsymbol{v}_h^n) &= \int_{t^{n-1}}^{t^n}\mathcal{R}_{1t}(\boldsymbol{v}_h^n)\,\mathrm{d}t\\ &\lesssim h\int_{t^{n-1}}^{t^n} M_{\boldsymbol{u}t}^{\frac12}\|\boldsymbol{v}_h^n\|_{a_1}\,\mathrm{d}t\\ &\le Ch^2\int_{t^{n-1}}^{t^n} M_{\boldsymbol{u}t}\,\mathrm{d}t+\frac{\Delta t}{8}\|\boldsymbol{v}_h^n\|_{a_1}^2,\end{aligned}$$

where we have used the inequality (22), the Cauchy-Schwarz inequality, and the fact $\boldsymbol{v}_h^n$ is constant with respect to the time t. The proof is completed. □

Lemma 4.2. *If $\boldsymbol{u}_{tt}\in L^2(\boldsymbol{H}(\mathrm{div}))$ and $p_{tt}\in L^2(L^2)$, we have*

$$\mathcal{R}_3^n(q_h^n)\le\int_{t^{n-1}}^{t^n}(\alpha\|\mathrm{div}\,\boldsymbol{u}_{tt}\|_0\|q_h^n\|_0+c_0\|p_{tt}\|_0\|q_h^n\|_0)\,\mathrm{d}t. \tag{39}$$

Moreover, by setting $q_h^n=\Delta t\,\theta_p^n$, we obtain

$$\mathcal{R}_3^n(\Delta t\,\theta_p^n)\le C\int_{t^{n-1}}^{t^n}((\Delta t)^2M_{tt}+h^2M_{\boldsymbol{u}})\,\mathrm{d}t+\frac{\Delta t}{8}\|\theta_{\boldsymbol{u}}^n\|_{a_1}^2+\frac{\Delta t\,c_0}{2}\|\theta_p^n\|_0^2, \tag{40}$$

where $M_{tt} := (\mu\|\mathrm{div}\,\boldsymbol{u}_{tt}\|_0^2+c_0\|p_{tt}\|_0^2)$.

Proof. It follows from the definition of $\mathcal{R}_3^n$ and Taylor's theorem that

$$\begin{aligned}\mathcal{R}_3^n(q_h^n) &= b_1(\delta_t\boldsymbol{u}^n-\boldsymbol{u}_t^n,q_h^n)+c_0(\delta_t p^n-p_t^n,q_h^n)\\ &=\alpha\left(\mathrm{div}(\boldsymbol{u}^n-\boldsymbol{u}^{n-1}-\Delta t\,\boldsymbol{u}_t^n),(\Delta t)^{-1}q_h^n\right)\\ &\quad + c_0(p^n-p^{n-1}-\Delta t\,p_t^n,(\Delta t)^{-1}q_h^n)\\ &=\int_{t^{n-1}}^{t^n}(t^{n-1}-t)\left(\alpha(\mathrm{div}\,\boldsymbol{u}_{tt}(t),(\Delta t)^{-1}q_h^n)+c_0(p_{tt}(t),(\Delta t)^{-1}q_h^n)\right)\mathrm{d}t\\ &\le\int_{t^{n-1}}^{t^n}(\alpha\|\mathrm{div}\,\boldsymbol{u}_{tt}(t)\|_0\|q_h^n\|_0+c_0\|p_{tt}(t)\|_0\|q_h^n\|_0)\,\mathrm{d}t.\end{aligned}$$

To obtain the inequality (40), we use Lemma 3.9, and thus have

$$\mathcal{R}_3^n(\Delta t\,\theta_p^n)\le\Delta t\int_{t^{n-1}}^{t^n}(\mu^{\frac12}\|\mathrm{div}\,\boldsymbol{u}_{tt}\|_0(\|\theta_{\boldsymbol{u}}^n\|_{a_1}+h(M_{\boldsymbol{u}}^n)^{\frac12})+c_0\|p_{tt}\|_0\|\theta_p^n\|_0)\,\mathrm{d}t.$$

Then the desired inequality is from the Cauchy-Schwarz inequality and the fact $\theta_{\boldsymbol{u}}^n$, θ_p^n are constants with respect to the time t. □

Theorem 4.3. *Let $(\boldsymbol{u},\boldsymbol{w},p)$ and $(\boldsymbol{u}_h^n,\boldsymbol{w}_h^n,p_h^n)$ be the unique solutions to (1) and (34) respectively. Assuming quasi-uniform of the mesh and sufficient regularity for the true solution, we have the following estimate:*

$$\begin{aligned}\max_{1\le n\le N}\left(\|\theta_{\boldsymbol{u}}^n\|_{a_1}^2+c_0\|\theta_p^n\|_0^2\right)+\Delta t\sum_{n=1}^N\|\theta_{\boldsymbol{w}}^n\|_{a_2}^2 &\lesssim (\Delta t)^2e^T\int_0^T M_{tt}\,\mathrm{d}t+\\ &\quad h^2e^T\left(\max_{1\le n\le N}M_{\boldsymbol{u}}^n+\int_0^T(M_{\boldsymbol{u}t}+M_{\boldsymbol{u}}+M_{\boldsymbol{w}})\,\mathrm{d}t\right).\end{aligned} \tag{41}$$

Proof. Setting $\boldsymbol{v}_h=\delta_t\theta_{\boldsymbol{u}}^n$, $\boldsymbol{z}_h=\theta_{\boldsymbol{w}}^n$, and $q_h=\theta_p^n$ in (35)-(37), we have

$$a_{h,1}(\theta_{\boldsymbol{u}}^n,\delta_t\theta_{\boldsymbol{u}}^n)+a_{h,2}(\theta_{\boldsymbol{w}}^n,\theta_{\boldsymbol{w}}^n)+a_{h,3}(\delta_t\theta_p^n,\theta_p^n)=\mathcal{R}_1^n(\delta_t\theta_{\boldsymbol{u}}^n)+\mathcal{R}_2^n(\theta_{\boldsymbol{w}}^n)+\mathcal{R}_3^n(\theta_p^n),$$

which, together with the definition δ_t and the Cauchy-Schwarz inequality, yields

$$\frac{1}{2}\|\theta_{\boldsymbol{u}}^n\|_{a_1}^2+\frac{c_0}{2}\|\theta_p^n\|_0^2+\Delta t\|\theta_{\boldsymbol{w}}^n\|_{a_2}^2 \le \frac{1}{2}\|\theta_{\boldsymbol{u}}^{n-1}\|_{a_1}^2+\frac{c_0}{2}\|\theta_p^{n-1}\|^2 + \mathcal{R}_1^n(\Delta t\,\delta_t\theta_{\boldsymbol{u}}^n)+\mathcal{R}_2^n(\Delta t\,\theta_{\boldsymbol{w}}^n)+\mathcal{R}_3^n(\Delta t\,\theta_p^n),$$

and therefore,

$$\frac{1}{2}\|\theta_{\boldsymbol{u}}^N\|_{a_1}^2+\frac{c_0}{2}\|\theta_p^N\|^2+\sum_{n=1}^N\Delta t\|\theta_{\boldsymbol{w}}^n\|_{a_2}^2 \le \sum_{n=1}^N \Delta t(\mathcal{R}_1^n(\delta_t\theta_{\boldsymbol{u}}^n)+\mathcal{R}_2^n\left(\theta_{\boldsymbol{w}}^n)+\mathcal{R}_3^n(\theta_p^n)\right), \quad (42)$$

where we have used the fact $\theta_{\boldsymbol{u}}^0=\mathbf{0}$, $\theta_p^0=0$.

For the first term in the right hand side of (42), we derive by directly calculation, the inequalities (20) and (38), and the Cauchy-Schwarz inequality, that

$$\begin{aligned}\sum_{n=1}^N\mathcal{R}_1^n(\Delta t\,\delta_t\theta_{\boldsymbol{u}}^n)&=\mathcal{R}_1^N(\theta_{\boldsymbol{u}}^N)-\sum_{n=2}^N(\mathcal{R}_1^n(\theta_{\boldsymbol{u}}^{n-1})-\mathcal{R}_1^{n-1}(\theta_{\boldsymbol{u}}^{n-1}))\\ &\lesssim h(M_{\boldsymbol{u}}^N)^{\frac{1}{2}}\|\theta_{\boldsymbol{u}}^N\|_{a_1}-\sum_{n=2}^N(\mathcal{R}_1^n(\theta_{\boldsymbol{u}}^{n-1})-\mathcal{R}_1^{n-1}(\theta_{\boldsymbol{u}}^{n-1}))\\ &\le Ch^2\left(M_{\boldsymbol{u}}^N+\int_0^T M_{\boldsymbol{u}t}\,\mathrm{d}t\right)+\frac{\Delta t}{8}\sum_{n=2}^N\|\theta_{\boldsymbol{u}}^{n-1}\|_{a_1}^2+\frac{1}{4}\|\theta_{\boldsymbol{u}}^N\|_{a_1}^2.\end{aligned}$$

For the second term in (42), we have from the inequality (21) that

$$\begin{aligned}\sum_{n=1}^N\mathcal{R}_2^n(\Delta t\,\theta_{\boldsymbol{w}}^n)&\lesssim\sum_{n=1}^N\Delta t\,h(M_{\boldsymbol{w}}^n)^{\frac{1}{2}}\|\theta_{\boldsymbol{w}}^n\|_{a_2}\le C\sum_{n=1}^N\Delta t\,h^2M_{\boldsymbol{w}}^n+\frac{\Delta t}{2}\sum_{n=1}^N\|\theta_{\boldsymbol{w}}^n\|_{a_2}^2\\ &\le Ch^2\int_0^T M_{\boldsymbol{w}}\,\mathrm{d}t+\frac{\Delta t}{2}\sum_{n=1}^N\|\theta_{\boldsymbol{w}}^n\|_{a_2}^2.\end{aligned}$$

For the last term in the right hand side of (42), Lemma 4.2 implies

$$\sum_{n=1}^N\mathcal{R}_3^n(\Delta t\,\theta_p^n)\le C\int_0^T((\Delta t)^2M_{tt}+h^2M_{\boldsymbol{u}})\,\mathrm{d}t+\Delta t\sum_{n=1}^N\left(\frac{1}{8}\|\theta_{\boldsymbol{u}}^n\|_{a_1}^2+\frac{c_0}{2}\|\theta_p^n\|_0^2\right).$$

Plugging the above three inequalities into (42), we have

$$\begin{aligned}&(\frac{1}{4}-\frac{\Delta t}{8})\|\theta_{\boldsymbol{u}}^N\|_{a_1}^2+(\frac{c_0}{2}-\frac{c_0\Delta t}{4})\|\theta_p^N\|_0^2+\frac{\Delta t}{2}\sum_{n=1}^N\|\theta_{\boldsymbol{w}}^n\|_{a_2}^2\\ &\le Ch^2\left(M_{\boldsymbol{u}}^N+\int_0^T(M_{\boldsymbol{u}t}+M_{\boldsymbol{u}}+M_{\boldsymbol{w}})\,\mathrm{d}t\right)+C\Delta t^2\int_0^T M_{tt}\,\mathrm{d}t\\ &+\frac{\Delta t}{4}\sum_{n=1}^{N-1}(\|\theta_{\boldsymbol{u}}^n\|_{a_1}^2+2c_0\|\theta_p^n\|_0^2).\end{aligned}$$

Therefore, the discrete Gronwall inequality leads to the inequality (41). □

5. Numerical experiments

In this section, we shall present some numerical experiments to verify our theoretical results.

5.1. Example 1

In this first numerical test, we consider the poroelastic equations in $\Omega=[0,1]^2$ with the time interval $[0,1]$. The source terms $\boldsymbol{f}_{\boldsymbol{u}}$, $\boldsymbol{f}_{\boldsymbol{w}}$, and f_p are chosen so that the exact solution $(\boldsymbol{u},\boldsymbol{w},p)$ is

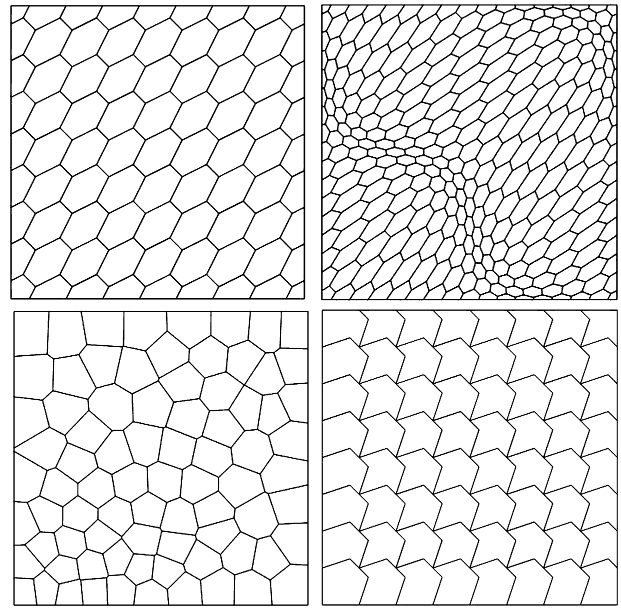

Fig. 1. Illustrations of meshes $\mathcal{T}^1$, $\mathcal{T}^2$, $\mathcal{T}^3$, $\mathcal{T}^4$.

$$\boldsymbol{u}(\boldsymbol{x},t)=t\begin{pmatrix}\sin(\pi x)\sin(\pi y)\\ x(1-x)y(1-y)\end{pmatrix},$$

$$\boldsymbol{w}(\boldsymbol{x},t)=\kappa\begin{pmatrix}0\\ \pi e^{-t}\sin(\pi y)\end{pmatrix},$$

$$p(\boldsymbol{x},t)=e^{-t}(1+\cos(\pi y)).$$

Let all the parameters in the equation (1) be unit. The tests are carried out on four types of meshes, that is, polygonal mesh $\mathcal{T}^1$ generated by the dual of the uniform triangle mesh, distorted polygonal mesh $\mathcal{T}^2$ by perturbing the interior nodes of $\mathcal{T}^1$, centroidal Voronoi mesh $\mathcal{T}^3$ using ten Lloyd's iterations [35], and non-convex mesh $\mathcal{T}^4$, respectively (see Fig. 1 for an illustration). The time step size is set to be equal to the meshsize.

In Tables 1–4, we list the errors in the displacement $\theta_{\boldsymbol{u}}^N$ measured by the discrete L^2 norm $\|\cdot\|_{0,h}$ and the energy norm $\|\cdot\|_{a_1}$, the errors in the velocity $\theta_{\boldsymbol{w}}^N$ with respect to $\|\cdot\|_{a_2}$ and $\|\operatorname{div}\cdot\|_0$, and the errors in the pressure θ_p^N and e_p^N under the L^2 norm, at the final time on progressively "refined meshes". Here,

$$\theta_{\boldsymbol{u}}^N:=\boldsymbol{I}_h^{\boldsymbol{V}}\boldsymbol{u}^N-\boldsymbol{u}_h^N,\ \theta_{\boldsymbol{w}}^N:=\boldsymbol{I}_h^{\boldsymbol{W}}\boldsymbol{w}^N-\boldsymbol{w}_h^N$$
$$\theta_p^N:=I_h^Qp^N-p_h^N,\ \ e_p^N:=p(T)-p_h^N,$$

and the discrete L^2 norm is defined for all $\boldsymbol{v}\in\boldsymbol{V}_h$ as

$$\|\boldsymbol{v}\|_{0,h}^2:=\sum_{E\in\mathcal{T}_h}\|\boldsymbol{\Pi}_E^o\boldsymbol{v}^{\mathrm{div}}\|_E^2+\|h^{\frac{1}{2}}\boldsymbol{\Pi}_{\partial E}\mathcal{J}_{\partial E}(\boldsymbol{v})\|_{\partial E}^2.$$

We also plot (in log-log scale) the errors with respect to the mesh sizes for different types of meshes in Figs. 2-3. We observe that the errors $\|e_p^N\|_0$ and $\|\theta_{\boldsymbol{u}}^N\|_{a_1}$ are of the order $O(h)$, while the errors $\|\theta_p^N\|_0$, $\|\theta_{\boldsymbol{w}}^N\|_{a_2}$, $\|\theta_{\boldsymbol{u}}^N\|_{0,h}$ are of the order $O(h^2)$. Superconvergence for the error $\|\operatorname{div}\theta_{\boldsymbol{w}}^N\|_0$ is observed on the three types of meshes except the centroidal Voronoi meshes.

5.2. Example 2

In the second example, we do the tests to show the dependence of our method with respect to the Lamé constant λ and the constrained specific storage coefficient c_0. On the square $[0,1]^2$ and the time interval $[0,1]$, the test solution reads as

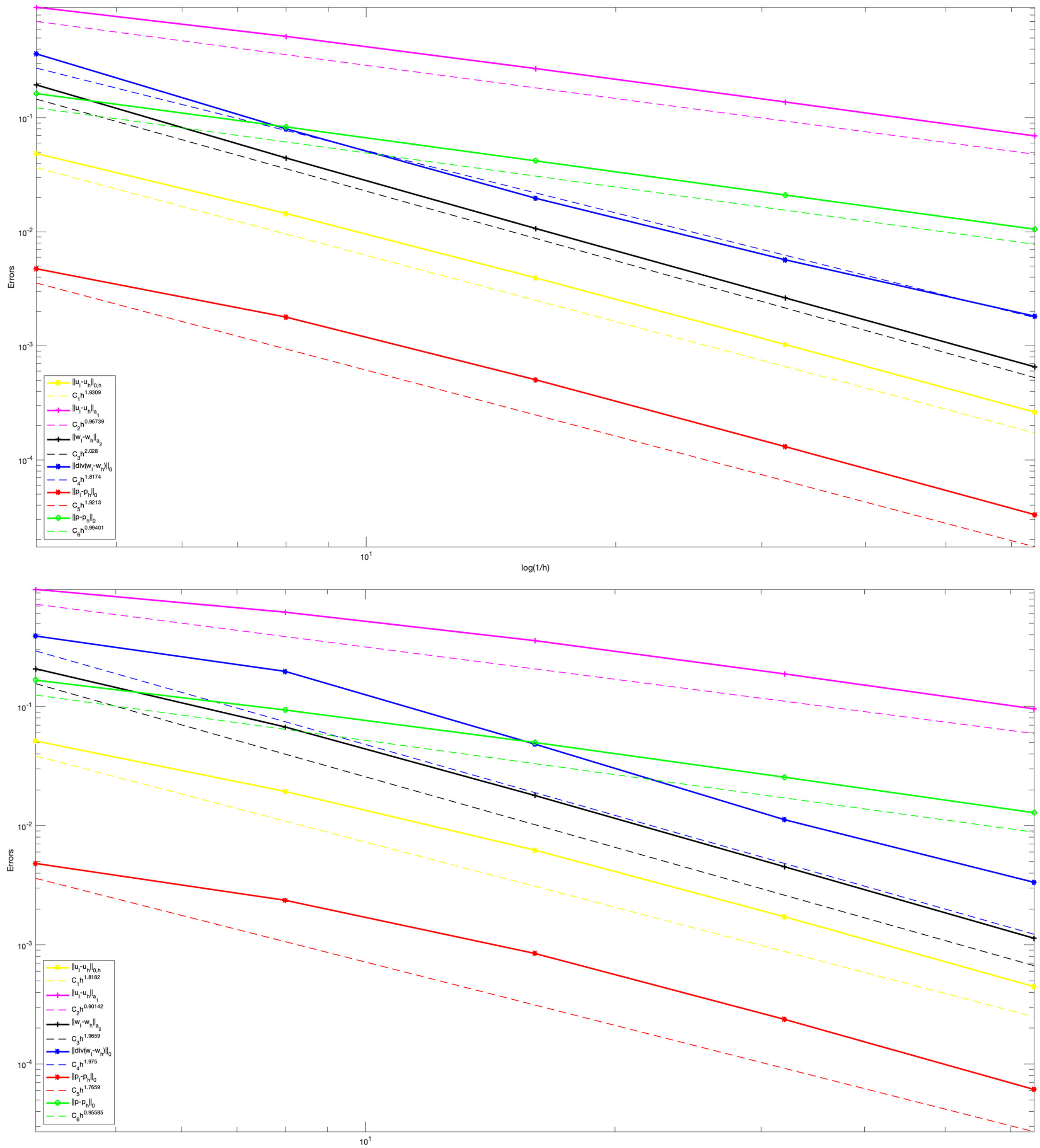

Fig. 2. The loglog plots of errors w.r.t the mesh sizes for the dual meshes $\mathcal{T}^1$ (left), for the distorted dual meshes $\mathcal{T}^2$ (right).

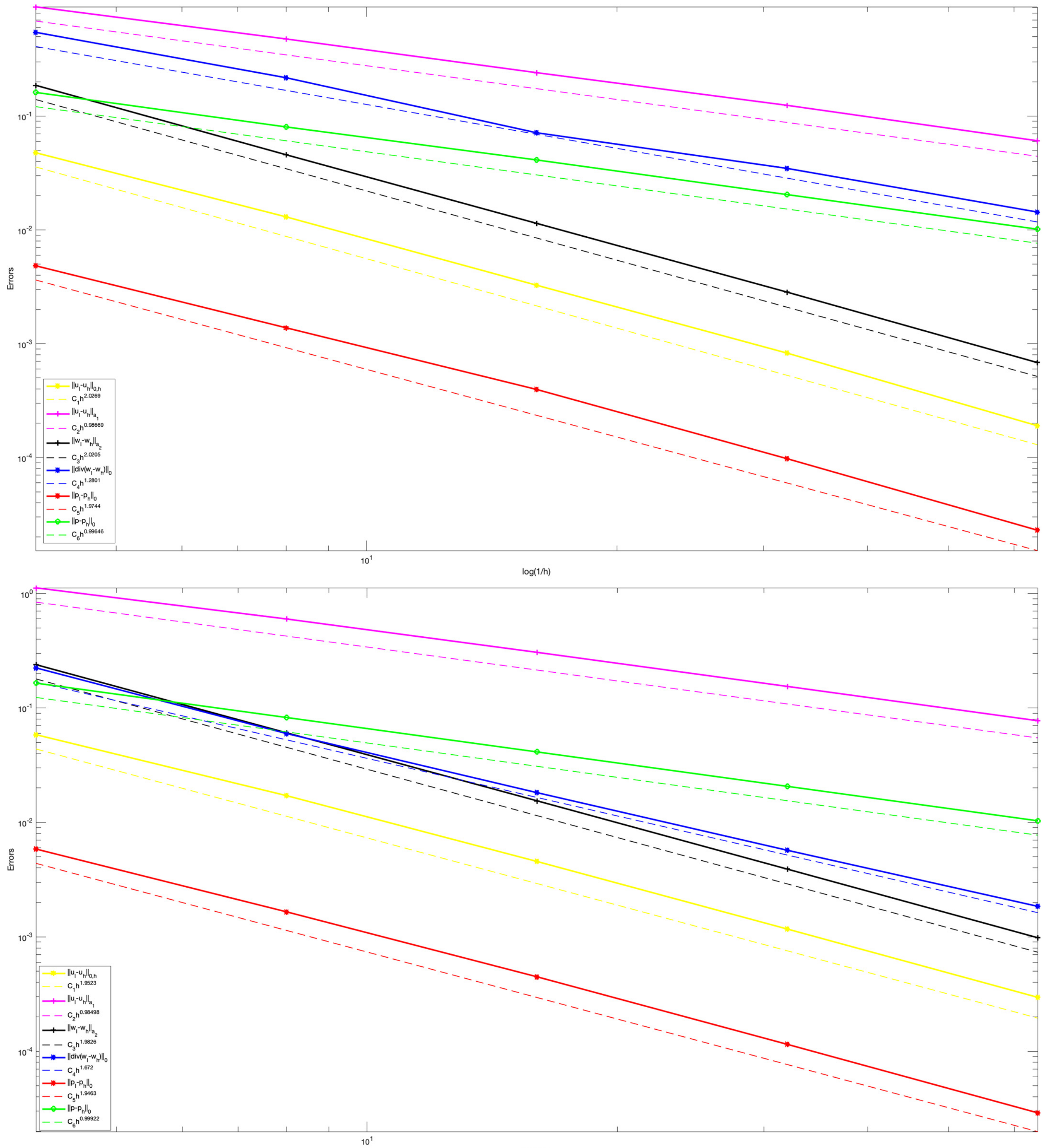

Fig. 3. The loglog plots of errors w.r.t the mesh sizes for the centroidal Voronoi meshes $\mathcal{T}^3$ (left), for the non-convex meshes $\mathcal{T}^4$ (right).

Table 1
The errors on the dual mesh $\mathcal{T}^1$.

h	$\|\|\theta_{\boldsymbol{u}}^N\|\|_{0,h}$	$\|\|\theta_{\boldsymbol{u}}^N\|\|_{a_1}$	$\|\|\theta_{\boldsymbol{w}}^N\|\|_{a_2}$	$\|\|\operatorname{div}\theta_{\boldsymbol{w}}^N\|\|_0$	$\|\|\theta_p^N\|\|_0$	$\|\|e_p^N\|\|_0$
2.50e-01	4.87e-02	9.35e-01	1.95e-01	3.64e-01	4.75e-03	1.63e-01
1.25e-01	1.45e-02	5.19e-01	4.45e-02	8.02e-02	1.79e-03	8.33e-02
6.25e-02	3.95e-03	2.71e-01	1.07e-02	1.97e-02	5.05e-04	4.20e-02
3.12e-02	1.03e-03	1.38e-01	2.64e-03	5.69e-03	1.31e-04	2.11e-02
1.56e-02	2.63e-04	6.95e-02	6.56e-04	1.82e-03	3.31e-05	1.05e-02

Table 2
The errors on the distorted dual mesh $\mathcal{T}^2$.

h	$\|\|\theta_{\boldsymbol{u}}^N\|\|_{0,h}$	$\|\|\theta_{\boldsymbol{u}}^N\|\|_{a_1}$	$\|\|\theta_{\boldsymbol{w}}^N\|\|_0$	$\|\|\operatorname{div}\theta_{\boldsymbol{w}}^N\|\|_0$	$\|\|\theta_p^N\|\|_0$	$\|\|e_p^N\|\|_0$
2.50e-01	5.14e-02	9.63e-01	2.08e-01	3.91e-01	4.82e-03	1.67e-01
1.25e-01	1.94e-02	6.20e-01	6.74e-02	1.97e-01	2.37e-03	9.36e-02
6.25e-02	6.24e-03	3.58e-01	1.79e-02	4.84e-02	8.47e-04	5.00e-02
3.12e-02	1.72e-03	1.88e-01	4.53e-03	1.12e-02	2.37e-04	2.55e-02
1.56e-02	4.46e-04	9.57e-02	1.14e-03	3.35e-03	6.12e-05	1.29e-02

Table 3
The errors on the centroidal Voronoi mesh $\mathcal{T}^3$.

h	$\|\|\theta_{\boldsymbol{u}}^N\|\|_{0,h}$	$\|\|\theta_{\boldsymbol{u}}^N\|\|_{a_1}$	$\|\|\theta_{\boldsymbol{w}}^N\|\|_0$	$\|\|\operatorname{div}\theta_{\boldsymbol{w}}^N\|\|_0$	$\|\|\theta_p^N\|\|_0$	$\|\|e_p^N\|\|_0$
2.50e-01	4.77e-02	9.12e-01	1.87e-01	5.45e-01	4.84e-03	1.61e-01
1.25e-01	1.30e-02	4.76e-01	4.58e-02	2.17e-01	1.38e-03	8.03e-02
6.25e-02	3.27e-03	2.41e-01	1.14e-02	7.14e-02	3.97e-04	4.12e-02
3.12e-02	8.28e-04	1.24e-01	2.84e-03	3.47e-02	9.78e-05	2.04e-02
1.56e-02	1.90e-04	6.07e-02	6.83e-04	1.44e-02	2.30e-05	1.01e-02

Table 4
The errors on the non-convex polygonal mesh ($\mathcal{T}^4$).

h	$\|\|\theta_{\boldsymbol{u}}^N\|\|_{0,h}$	$\|\|\theta_{\boldsymbol{u}}^N\|\|_{a_1}$	$\|\|\theta_{\boldsymbol{w}}^N\|\|_0$	$\|\|\operatorname{div}\theta_{\boldsymbol{w}}^N\|\|_0$	$\|\|\theta_p^N\|\|_0$	$\|\|e_p^N\|\|_0$
2.50e-01	5.84e-02	1.12e+00	2.39e-01	2.24e-01	5.85e-03	1.65e-01
1.25e-01	1.71e-02	5.99e-01	6.06e-02	5.98e-02	1.66e-03	8.25e-02
6.25e-02	4.56e-03	3.06e-01	1.55e-02	1.82e-02	4.48e-04	4.13e-02
3.12e-02	1.17e-03	1.54e-01	3.91e-03	5.71e-03	1.15e-04	2.07e-02
1.56e-02	2.96e-04	7.73e-02	9.83e-04	1.85e-03	2.90e-05	1.03e-02

Table 5
The errors for different Lamé constant λ on the dual mesh ($\mathcal{T}^1$).

λ	h	$\|\|\theta_{\boldsymbol{u}}^N\|\|_{0,h}$	$\|\|\theta_{\boldsymbol{u}}^N\|\|_{a_1}$	$\|\|\theta_{\boldsymbol{w}}^N\|\|_{a_2}$	$\|\|\operatorname{div}\theta_{\boldsymbol{w}}^N\|\|_0$	$\|\|\theta_p^N\|\|_0$	$\|\|e_p^N\|\|_0$
1e2	2.50e-01	3.96e-02	1.96e+00	4.28e-01	1.39e-01	7.80e-02	3.67e-01
	1.25e-01	9.32e-03	1.15e+00	1.21e-01	6.68e-02	2.80e-02	2.08e-01
	6.25e-02	2.55e-03	6.08e-01	3.24e-02	2.95e-02	7.67e-03	1.10e-01
	3.13e-02	7.05e-04	3.11e-01	8.48e-03	1.35e-02	1.85e-03	5.61e-02
1e8	2.50e-01	3.96e-02	1.96e+00	4.28e-01	1.37e-01	7.81e-02	3.67e-01
	1.25e-01	9.32e-03	1.15e+00	1.21e-01	6.61e-02	2.80e-02	2.08e-01
	6.25e-02	2.55e-03	6.08e-01	3.23e-02	2.93e-02	7.70e-03	1.10e-01
	3.12e-02	7.05e-04	3.11e-01	8.47e-03	1.34e-02	1.87e-03	5.61e-02

$$\boldsymbol{u}(x,t) = e^t\begin{pmatrix} \sin(\pi x)\cos(\pi y) \\ -\cos(\pi x)\sin(\pi y)\end{pmatrix} + \frac{e^t}{2\lambda}\begin{pmatrix} x^2 \\ y^2\end{pmatrix},$$

$$\boldsymbol{w} = -\kappa\nabla p, \quad p(x,t) = e^t(\sin(\pi x)\sin(\pi y) - 4/\pi^2).$$

5.2.1. Tests for the Lamé constant λ

To test the robustness with respect to λ, we set all the parameters to be 1 except the Lamé constant λ. In Table 5, we list the errors on the dual mesh $\mathcal{T}^1$ with respect two different λ. It is shown that the errors are almost the same on the same mesh and will not be deteriorated when λ becomes larger.

We also do the tests using the P2-RT0-P0 finite element approximation for $\lambda = 10^2$ and $\lambda = 10^8$ respectively. The errors are reported in Table 6. It is viewed that the error $\|\theta_{\boldsymbol{u}}^N\|_{a_1}$ depends on λ.

5.2.2. Tests for the parameter c_0

We then fix $\mu = \lambda = \alpha = \kappa = 1$ and do tests for $c_0 = 1e{-2}$ and $c_0 = 1e{-6}$ respectively. By comparing the results in Table 7, the errors do not depend on c_0. If P2-RT0-P0 element is used for the discretization, it seems the decay of the error $\|\theta_p^N\|_0$ is of $O(h^{0.75})$ from Table 8.

5.3. Example 3

In order to show the performance of nonphysical pressure oscillations, we test the cantilever bracket problem (see, e.g., [38]). The problem is defined on a unit square $[0,1]^2$. The boundary conditions are imposed as follows. The displacement is set to be zero at the left side $x = 0$, and a traction boundary condition is used at the other sides, i.e., $(\sigma(\boldsymbol{u}) - \alpha p\mathbb{I})\boldsymbol{n} = [0,-1]^\tau$ for $y = 1$, and $(\sigma(\boldsymbol{u}) - \alpha p\mathbb{I})\boldsymbol{n} = [0,-1]^\tau$ for the sides $y = 0$ and $x = 1$. The outer normal component of the flow velocity is assumed to be zero on the entire boundary. The material parameters is set as $\alpha = 0.93$, $c_0 = 0$, $\kappa = 10^{-7}$, $E = 10^5$, $\nu = 0.4$. All the other datas, including the loads and the initial conditions, are assumed to be zeros. In Fig. 4, we plot the numerical pressure at the first step ($\Delta t = 0.001$). It is observed that there is no spurious oscillations.

Table 6
The errors for different Lamé constant λ using the P2-RT0-P0 element.

λ	h	$\|\theta_{\boldsymbol{u}}^N\|_{0,h}$	$\|\theta_{\boldsymbol{u}}^N\|_{a_1}$	$\|\theta_{\boldsymbol{w}}^N\|_{a_2}$	$\|\operatorname{div}\theta_{\boldsymbol{w}}^N\|_0$	$\|\theta_p^N\|_0$	$\|e_p^N\|_0$
$1e2$	2.50e-01	1.13e-02	3.60e-01	2.52e-02	5.20e-04	2.86e-03	2.57e-03
	1.25e-01	1.74e-03	7.62e-02	6.45e-03	7.18e-05	6.63e-04	6.59e-04
	6.25e-02	1.79e-04	1.29e-02	1.68e-03	9.31e-06	1.22e-04	1.66e-04
	3.12e-02	1.37e-05	1.94e-03	4.77e-04	1.18e-06	2.11e-05	4.15e-05
$1e8$	2.50e-01	1.48e-02	4.01e+02	2.52e-02	5.25e-04	2.88e-03	2.57e-03
	1.25e-01	3.57e-03	1.04e+02	6.45e-03	7.20e-05	6.72e-04	6.59e-04
	6.25e-02	8.83e-04	2.63e+01	1.68e-03	9.31e-06	1.26e-04	1.66e-04
	3.12e-02	2.20e-04	6.58e+00	4.72e-04	1.18e-06	2.09e-05	4.15e-05

Table 7
The errors for different c_0 on the dual mesh ($\mathcal{T}^1$).

c_0	h	$\|\theta_{\boldsymbol{u}}^N\|_{0,h}$	$\|\theta_{\boldsymbol{u}}^N\|_{a_1}$	$\|\theta_{\boldsymbol{w}}^N\|_{a_2}$	$\|\operatorname{div}\theta_{\boldsymbol{w}}^N\|_0$	$\|\theta_p^N\|_0$	$\|e_p^N\|_0$
$1e{-}2$	2.50e-01	5.74e-03	2.75e-01	5.87e-02	5.76e-02	9.40e-03	4.94e-02
	1.25e-01	1.41e-03	1.60e-01	1.70e-02	2.68e-02	3.22e-03	2.81e-02
	6.25e-02	3.84e-04	8.47e-02	4.88e-03	1.29e-02	7.25e-04	1.48e-02
	3.12e-02	1.04e-04	4.33e-02	1.58e-03	6.34e-03	9.29e-05	7.59e-03
$1e{-}6$	2.50e-01	5.74e-03	2.75e-01	5.87e-02	5.76e-02	9.40e-03	4.94e-02
	1.25e-01	1.41e-03	1.60e-01	1.70e-02	2.69e-02	3.22e-03	2.81e-02
	6.25e-02	3.84e-04	8.47e-02	4.87e-03	1.29e-02	7.26e-04	1.48e-02
	3.12e-02	1.04e-04	4.33e-02	1.57e-03	6.34e-03	9.33e-05	7.59e-03

Table 8
The errors for $c_0 = 1e{-}6$ using the P2-RT0-P0 element.

h	$\|\theta_{\boldsymbol{u}}^N\|_{0,h}$	$\|\theta_{\boldsymbol{u}}^N\|_{a_1}$	$\|\theta_{\boldsymbol{w}}^N\|_{a_2}$	$\|\operatorname{div}\theta_{\boldsymbol{w}}^N\|_0$	$\|\theta_p^N\|_0$	$\|e_p^N\|_0$
1.25e-01	3.03e-04	1.44e-02	7.91e-03	2.86e-04	4.05e-04	6.59e-04
6.25e-02	6.59e-05	6.93e-03	2.79e-03	3.50e-05	3.10e-04	1.66e-04
3.12e-02	1.47e-05	3.47e-03	1.20e-03	4.33e-06	1.96e-04	4.15e-05
1.56e-02	3.21e-06	1.74e-03	5.69e-04	5.39e-07	1.09e-04	1.04e-05

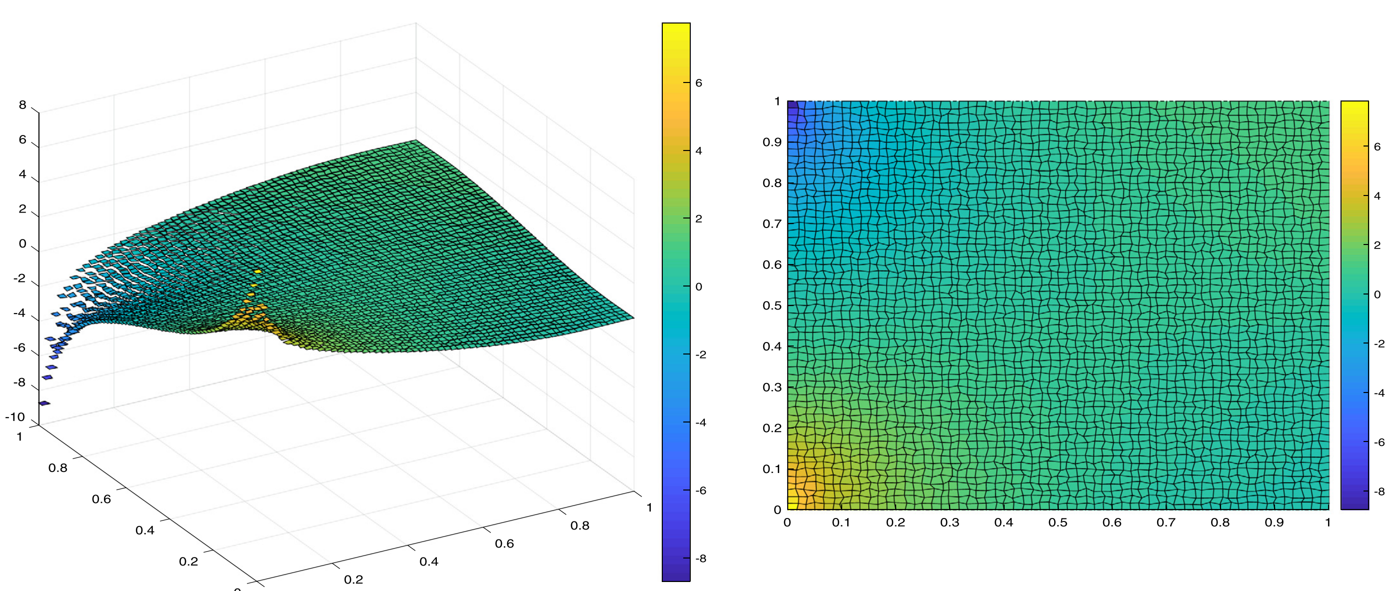

Fig. 4. The numerical pressure at $T = 0.001$ for the cantilever bracket problem.

Data availability

Data will be made available on request.

References

[1] P.F. Antonietti, L. Beirão da Veiga, D. Mora, M. Verani, A stream virtual element formulation of the Stokes problem on polygonal meshes, SIAM J. Numer. Anal. 52 (1) (2014) 386–404.
[2] T. Baerland, J.J. Lee, K.A. Mardal, R. Winther, Weakly imposed symmetry and robust preconditioners for Biot's consolidation model, Comput. Methods Appl. Math. 17 (3) (2017) 377–396.
[3] M. Bause, F. Radu, U. Köcher, Space–time finite element approximation of the Biot poroelasticity system with iterative coupling, Comput. Methods Appl. Mech. Eng. 320 (2017) 745–768.
[4] L. Beirão da Veiga, F. Brezzi, A. Cangiani, G. Manzini, L.D. Marini, A. Russo, Basic principles of virtual element methods, Math. Models Methods Appl. Sci. 23 (01) (2013) 199–214.
[5] L. Beirão da Veiga, F. Brezzi, L.D. Marini, A. Russo, H(div) and H(curl)-conforming virtual element methods, Numer. Math. 133 (2) (2016) 303–332.
[6] L. Berger, R. Bordas, D. Kay, S. Tavener, Stabilized lowest-order finite element approximation for linear three-field poroelasticity, SIAM J. Sci. Comput. 37 (5) (2015) A2222–A2245.
[7] D. Boffi, M. Botti, D.A. Di Pietro, A nonconforming high-order method for the Biot problem on general meshes, SIAM J. Sci. Comput. 38 (3) (2016) A1508–A1537.
[8] F. Brezzi, R.S. Falk, L.D. Marini, Basic principles of mixed virtual element methods, ESAIM: Math. Model. Numer. Anal. 48 (4) (2014) 1227–1240.
[9] R. Bürger, S. Kumar, D. Mora, R. Ruiz-Baier, N. Verma, Virtual element methods for the three-field formulation of time-dependent linear poroelasticity, Adv. Comput. Math. 47 (1) (2021) 2.
[10] L. Chen, F. Wang, A divergence free virtual element method for the Stokes problem on polyhedral meshes, J. Sci. Comput. 78 (2) (2019) 864–886.
[11] L. Chen, H. Wei, M. Wen, An interface-fitted mesh generator and virtual element methods for elliptic interface problems, J. Comput. Phys. 334 (1) (2017) 327–348.
[12] W. Chen, Y. Wang, Minimal degree H(curl) and H(div) conforming finite elements on polytopal meshes, Math. Comput. 86 (307) (2017) 2053–2087.
[13] J. Coulet, I. Faille, V. Girault, N. Guy, F. Nataf, A fully coupled scheme using virtual element method and finite volume for poroelasticity, Comput. Geosci. 24 (2020) 381–403.
[14] D.A. Di Pietro, A. Ern, A hybrid high-order locking-free method for linear elasticity on general meshes, Comput. Methods Appl. Mech. Eng. 283 (2015) 1–21.
[15] X. Feng, Z. Ge, Y. Li, Analysis of a multiphysics finite element method for a poroelasticity model, IMA J. Numer. Anal. 38 (1) (2017) 330–359.
[16] J.B. Haga, H. Osnes, H.P. Langtangen, On the causes of pressure oscillations in low-permeable and low-compressible porous media, Int. J. Numer. Anal. Methods Geomech. 36 (2012) 1507–1522.
[17] Q. Hong, J. Kraus, Parameter-robust stability of classical three-field formulation of Biot's consolidation model, Electron. Trans. Numer. Anal. 48 (2018) 202–226.
[18] X. Hu, C. Rodrigo, F.J. Gaspar, L.T. Zikatanov, A nonconforming finite element method for the Biot's consolidation model in poroelasticity, J. Comput. Appl. Math. 310 (2017) 143–154.
[19] J.J. Lee, Robust error analysis of coupled mixed methods for Biot's consolidation model, J. Sci. Comput. 69 (2) (2016) 610–632.
[20] J.J. Lee, K.A. Mardal, R. Winther, Parameter-robust discretization and preconditioning of Biot's consolidation model, SIAM J. Sci. Comput. 39 (1) (2017) A1–A24.
[21] K. Lipnikov, G. Manzini, M. Shashkov, Mimetic finite difference method, J. Comput. Phys. 257 (2014) 1163–1227.
[22] A. Mikelić, M.F. Wheeler, Convergence of iterative coupling for coupled flow and geomechanics, Comput. Geosci. 17 (3) (2013) 455–461.
[23] L. Mu, J. Wang, X. Ye, Weak Galerkin finite element methods on polytopal meshes, Int. J. Numer. Anal. Model. 12 (1) (2015) 31–53.
[24] C. Niu, H. Rui, X. Hu, A stabilized hybrid mixed finite element method for poroelasticity, Comput. Geosci. 25 (2) (2021) 757–774.
[25] R. Oyarzúa, R. Ruiz-Baier, Locking-free finite element methods for poroelasticity, SIAM J. Numer. Anal. 54 (5) (2016) 2951–2973.
[26] P.J. Phillips, M.F. Wheeler, A coupling of mixed and continuous Galerkin finite element methods for poroelasticity i: the continuous in time case, Comput. Geosci. 11 (2) (2007) 131–144.
[27] P.J. Phillips, M.F. Wheeler, A coupling of mixed and continuous Galerkin finite element methods for poroelasticity ii: the discrete-in-time case, Comput. Geosci. 11 (2) (2007) 145–158.
[28] P.J. Phillips, M.F. Wheeler, A coupling of mixed and discontinuous Galerkin finite-element methods for poroelasticity, Comput. Geosci. 12 (4) (2008) 417–435.
[29] P.J. Phillips, M.F. Wheeler, Overcoming the problem of locking in linear elasticity and poroelasticity: an heuristic approach, Comput. Geosci. 13 (2009) 5–12.
[30] M. Preisig, J.H. Prévost, Stabilization procedures in coupled poromechanics problems: a critical assessment, Int. J. Numer. Anal. Methods Geomech. 35 (11) (2011) 1207–1225.
[31] C. Rodrigo, Poroelasticity problem: numerical difficulties and efficient multigrid solution, SeMA 73 (2016) 31–57.
[32] C. Rodrigo, F. Gaspar, X. Hu, L. Zikatanov, Stability and monotonicity for some discretizations of the Biot's consolidation model, Comput. Methods Appl. Mech. Eng. 298 (2016) 183–204.
[33] C. Rodrigo, X. Hu, P. Ohm, J. Adler, F. Gaspar, L. Zikatanov, New stabilized discretizations for poroelasticity and the Stokes' equations, Comput. Methods Appl. Mech. Eng. 341 (2018) 467–484.
[34] M. Sun, H. Rui, A coupling of weak Galerkin and mixed finite element methods for poroelasticity, Comput. Math. Appl. 73 (5) (2017) 804–823.
[35] C. Talischi, G.H. Paulino, A. Pereira, I.F. Menezes, PolyMesher: a general-purpose mesh generator for polygonal elements written in Matlab, Struct. Multidiscip. Optim. 45 (2012) 309–328.
[36] X. Tang, Z. Liu, B. Zhang, M. Feng, On the locking-free three-field virtual element methods for Biot's consolidation model in poroelasticity, ESAIM: M2AN 55 (2021) S909–S939.
[37] J. Wang, X. Ye, A weak Galerkin finite element method for second-order elliptic problems, J. Comput. Appl. Math. 241 (2013) 103–115.
[38] S.-Y. Yi, A coupling of nonconforming and mixed finite element methods for Biot's consolidation model, Numer. Methods Partial Differ. Equ. 29 (5) (2013) 1749–1777.
[39] S.-Y. Yi, Convergence analysis of a new mixed finite element method for Biot's consolidation model, Numer. Methods Partial Differ. Equ. 30 (4) (2014) 1189–1210.
[40] S.-Y. Yi, A study of two modes of locking in poroelasticity, SIAM J. Numer. Anal. 55 (4) (2017) 1915–1936.